AEDC-TR-83-6

C # H

Collison Numbers in Expanding Conical Nozzle Flow Fields

J. W. Lewis and M. S. Smith
Calspan Field Services, Inc.

February 1983

Final Report for Period October 1, 1979 to August 1, 1980

**ARNOLD ENGINEERING DEVELOPMENT CENTER
ARNOLD AIR FORCE STATION, TENNESSEE
AIR FORCE SYSTEMS COMMAND
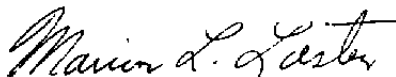UNITED STATES AIR FORCE**

APPROVAL STATEMENT

This report has been reviewed and approved.

MARSHALL K. KINGERY
Directorate of Technology
Deputy for Operations

Approved for publication:

FOR THE COMMANDER

MARION L. LASTER
Director of Technology
Deputy for Operations

REPORT DOCUMENTATION PAGE		READ INSTRUCTIONS BEFORE COMPLETING FORM
1 REPORT NUMBER AEDC-TR-83-6	2 GOVT ACCESSION NO.	3 RECIPIENT'S CATALOG NUMBER
4. TITLE *(and Subtitle)* COLLISION NUMBERS IN EXPANDING CONICAL NOZZLE FLOW FIELDS		5 TYPE OF REPORT & PERIOD COVERED Final Report–October 1, 1979 to August 1, 1980
		6 PERFORMING ORG REPORT NUMBER
7 AUTHOR*(s)* J. W. L. Lewis and M. S. Smith, Calspan Field Services, Inc.		8 CONTRACT OR GRANT NUMBER*(s)*
9 PERFORMING ORGANIZATION NAME AND ADDRESS Arnold Engineering Development Center/DOT Air Force Systems Command Arnold Air Force Station, Tennessee 37389		10 PROGRAM ELEMENT, PROJECT, TASK AREA & WORK UNIT NUMBERS Program Element 61102F
11 CONTROLLING OFFICE NAME AND ADDRESS Arnold Engineering Development Center/DOS Air Force Systems Command Arnold Air Force Station, Tennessee 37389		12 REPORT DATE February 1983
		13 NUMBER OF PAGES 58
14 MONITORING AGENCY NAME & ADDRESS*(If different from Controlling Office)*		15 SECURITY CLASS *(of this report)* UNCLASSIFIED
		15a DECLASSIFICATION/DOWNGRADING SCHEDULE N/A

16 DISTRIBUTION STATEMENT *(of this Report)*

Approved for public release; distribution unlimited.

17. DISTRIBUTION STATEMENT *(of the abstract entered in Block 20, if different from Report)*

18 SUPPLEMENTARY NOTES

Available in Defense Technical Information Center (DTIC)

19 KEY WORDS *(Continue on reverse side if necessary and identify by block number)*

collisions	reservoir	gas flow	temperature
interaction	parameter	flow fields	impact
potential	Mach Number	coefficients	nozzle
molecular	integrals	elastic	moment
scaling	free stream	density	ratio

20 ABSTRACT *(Continue on reverse side if necessary and identify by block number)*

    The cumulative elastic collision number has been calculated for the supersonic region of isentropic, continuum conical nozzle flow fields for gaseous species characterized by the specific heat ratios γ = 5/3, 7/5, and 9/7. The cumulative collision number was determined as a function of Mach number and axial distance parameter $\hat{x} \tan \theta$, the latter specialized to the nozzle half-angles θ = 5, 10.5, and 15 deg. The calculations were extended to study the effects of the type of intermolecular potential interaction on

20. ABSTRACT (Continued)

the cumulative collision number. Specifically, the interaction potentials investigated included the attractive inverse $-r^6$, the Lennard-Jones 12:6, the Stockmayer and Krieger 12:6:3 potentials, and the hard-sphere interaction. The results have been presented in nondimensional form in terms of the characteristic well-depth energies and ranges of the intermolecular potentials, and the range of the nondimensional reservoir temperature studied was $2 < T_o^* < 10$, which corresponds to the range of approximately 200 to 1000 K for typical nonpolar molecular species. The results obtained for the inverse $-r$ potential using a close-encounter collision model allowed simple scaling of the results with reservoir temperature which was not possible for the two- and three-term potentials. Quantitative comparisons of the results are presented.

PREFACE

The work reported herein was conducted by the Arnold Engineering Development Center (AEDC), Air Force Systems Command (AFSC) for the Air Force Rocket Propulsion Laboratory (AFRPL) Edwards AFB, CA. Dr. David Mann was the AFRPL project monitor. The research was begun by ARO, Inc., AEDC Division, operating contractor for the AEDC, and completed by Calspan Field Services, Inc., AEDC Division, operating contractor for the aerospace flight dynamics testing at AEDC, AFSC, Arnold Air Force Station, Tennessee, under Project No. P34M-19. Co-author M. S. Smith is a research assistant at the University of Tennessee Space Institute. The manuscript was submitted for publication on November 3, 1981.

CONTENTS

ILLUSTRATIONS

Figure

1.0 INTRODUCTION

The continuum flow-field expansion of molecular species provides the environment and stimulus for a variety of interesting, and sometimes complicated, intermolecular collisional phenomena. These phenomena include such processes as vibrational and rotational relaxation, chemical reactions, and condensation processes. The prediction of the effects of these collision processes on the gas-dynamic parameters of the flow field is of importance for a variety of application areas. Some exemplary application areas include providing flow fields of known properties for calibration purposes, the design of mass-sampling probes, the formation of continuum molecular beams, and the prediction of radiation signatures of exhaust plumes. An accurate prediction, however, requires knowledge of the state-specific molecular species distribution functions which are, in general, quite difficult to calculate. Fortunately, for many applications such accuracy is not required, but, rather, it is necessary only that an order-of-magnitude estimate be obtained for the effect of the relevant intermolecular collision processes.

For static gases, one approach to obtain such order-of-magnitude estimates is the calculation of the appropriate elastic collision rate coefficient which is adjusted by multiplication by the average transition probability for collision for the type of collisional process of interest. For expansion flow fields, this computation is complicated, for not only are the elastic collision rate coefficient and the inelastic collision transition probabilities both dependent on density and temperature, but now the density and temperature of the flow field are functions of the gas reservoir properties, the nozzle (or expansion source), geometrical characteristics, and the spatial coordinates of the flow field. As a result, specification of the average number of collisions or transitions experienced by a molecule in traversing a specified region of the flow field requires numerical integration of the density- and temperature-dependent rate coefficients over the specified expansion flow-field region.

The computation of the average elastic collision number experienced by a molecule in an expansion flow field is, in itself, of interest, for it is known that a variety of inelastic collision processes occur with collisional energy transfer probabilities which are of the same order of magnitude as those for elastic collisions. Such inelastic processes include rotational energy transfer, some chemical reactions, the quenching collisions of optical fluorescence, and optical line-broadening or phase-interrupting collisions. These computations have been performed, and the results are presented in this report. Specifically, the supersonic region of conical nozzle expansions has been investigated for flow fields of molecular constituents which interact with a variety of intermolecular potentials. The required numerical integrations were performed for collisions characterized by the hard-sphere potential, attractive inverse $-r^n$ potentials for $n = 3$ and 6, the two-term Lennard-Jones 12:6 potential, and the 12:6:3 Stockmayer and Krieger potentials.

Computations were performed to determine the average cumulative collision number of a molecule in traversing a specified region of the flow field, and the results demonstrate the effects on this collision number of the gas reservoir parameters, nozzle geometry and type of assumed interaction potential. Finally, the results are presented in a graphical form useful both for easy estimation of the effects of intermolecular collisions for a variety of application areas and for determination of the importance of accuracy in the representation or selection of the intermolecular potential function.

2.0 THEORY

2.1 COLLISION RATE FORMULATION

The gas sample of equilibrium temperature T is assumed to consist of two species, each of which is characterized by the classical Maxwell-Boltzmann distribution function (Ref. 1)

$$f_\alpha(\vec{v_i}) = (m_\alpha/2\pi k_B T)^{3/2} \exp[-(m_\alpha/2k_B T)\vec{v_\alpha} \cdot \vec{v_\alpha}] \tag{1}$$

where α designates the species of mass m_α; i, the Cartesian component; and $\vec{v_\alpha}$ is the velocity of species α relative to an origin which moves with the gas flow velocity. Defining $\widehat{\widehat{Z}}$ to be the number of collisions per second per unit volume of the gas sample,

$$d^7\widehat{\widehat{Z}} = \xi \cdot n_1 n_2(2\pi b\ db)[(m_1/2\pi k_B T)(m_2/2\pi k_B T)]^{3/2} v_r \cdot$$
$$\exp[-(m_1\vec{v_1} \cdot \vec{v_1} + m_2\vec{v_2} \cdot \vec{v_2})/2k_B T]\,d\vec{v_1}\,d\vec{v_2} \tag{2}$$

where n_i is the local number density of species i

$$v_r = |\vec{v_r}| = |\vec{v_1} - \vec{v_2}|$$

b is the impact parameter of the collision and

$$\xi = 1 \quad i \neq j$$
$$= \tfrac{1}{2} \quad i = j$$

Finally, $d^7\widehat{\widehat{Z}}$ designates the differential to be of 7th order.

The transformation from $(\vec{v_1}, \vec{v_2})$ velocity space to the center-of-mass variables $(\vec{v_c}, \vec{v_r})$ is simply effected, and since the transformation Jacobian is unity, one finds, after integration over the unimportant center-of-mass velocity vector $\vec{v_c}$,

$$d^4Z = \xi n_1 n_2(2\pi b\ db)(m_{12}/2\pi k_B T)^{3/2} \cdot v_r \exp(-m_{12}\vec{v_r} \cdot \vec{v_r}/2k_B T)d\vec{v_r} \tag{3}$$

where m_{12} is the reduced mass of species "1" and "2". Therefore, the collision frequency $\widehat{Z}$ for atom, or molecule, of type "1" with type "2" species is given by Refs. 1 and 2:

$$\widehat{Z} = \xi n_1 (m_{12}/2\pi k_B T)^{3/2} \int\int\int_{-\infty}^{\infty} d\vec{v_r} \, v_r \exp\left(-m_{12}v_r^2/2k_B T\right) \int_0^{\infty} db \, 2\pi b \qquad (4)$$

Considering only spherically symmetric intermolecular potential functions, $\phi(r)$, it is convenient to define the speed-dependent cross section $\sigma(v)$ to be

$$\sigma(v) = 2\pi \int_0^{\infty} b \, db \qquad (5)$$

and to transform the $\vec{v}$ space integrals of Eq. (4) to spherical v coordinates. Consequently, one finds

$$\widehat{Z} = \xi \cdot n_2 \cdot K(T) \qquad (6)$$

where the temperature-dependent, density-independent rate coefficient $K(T)$ is defined to be

$$K(T) = 4\pi (m_{12}/2\pi k_B T)^{3/2} \int_0^{\infty} dv \, \sigma(v) \, v^3 \exp\left(-m_{12}v^2/2k_B T\right) \qquad (7)$$

which, perhaps, assumes a more familiar form when written as

$$K(T) = \int_0^{\infty} dv \, \sigma(v) \, v \cdot f(v) \qquad (8)$$

For collisions described by a hard-sphere (HS) potential

$$\phi(r) = \infty \quad r \leq d$$
$$= 0 \quad r > d$$

it is seen that

$$\widehat{Z} = \xi \cdot n_2 \cdot (8RT/\pi \overline{M}_{12})^{1/2} \cdot \pi d_{12}^2 \qquad (9)$$

where $\overline{M}_{12}$ is the reduced gram molecular weight and R is the universal gas constant. The cross section $\sigma = \pi d_{12}^2$ is, of course, v-independent, and the collision diameter d_{12} is given by

$$d_{12} = (d_1 + d_2)/2$$

If the gas is composed of a single species, one obtains the even more familiar form

$$\widehat{Z} = 2n(\pi d^2)(RT/\pi \overline{M})^{1/2} \qquad (10)$$

7

where $\overline{M}$ is the gram molecular weight.

Clearly,

$$K(T)_{HS} = 2\sigma(RT/\pi\overline{M})^{1/2} \tag{11}$$

The formulation culminating in Eq. (11) can be generalized easily to describe mixtures of multiple species. If the ordered subscript pair (i,j) denotes an i-species specific parameter resulting from j-species interactions, it is seen that

$$\widehat{Z}_{i.} = \sum_j \widehat{Z}_{ij} \tag{12}$$

where

$$\widehat{Z}_{ij} = n_j K_{ij}(T) \tag{13a}$$

$$K_{ij}(T) = 4\pi(\overline{m}_{ij}/2\pi k_B T)^{3/2} \int_0^\infty dv\, \sigma_{ij}\, v^3 \exp(-\overline{m}_{ij}v^2/2k_B T) \tag{13b}$$

and

$$1/\overline{m}_{ij} = (1/m_i) + (1/m_j) \tag{13c}$$

2.2 CONVERSION TO FLOW COORDINATES

The conversion of the preceding collision rate expressions to flow coordinates is effected most conveniently by using the relation

$$dx = u_\infty dt$$

where u_∞ represents the flow speed; t, the time; and x, the axial flow-field coordinate.

For the conical nozzle source of throat diameter D it is convenient to define a nondimensional distance to be

$$\hat{x} = x/D$$

For the isentropic conical nozzle expansion one now finds

$$dZ_i/d\hat{x} = n_{T_0}D[<\overline{M}>/\gamma RT_0]^{1/2} \cdot (1/M) \cdot \{1 + [(\gamma-1)/2] M^2\}^{(\gamma-3)/2(\gamma-1)} \cdot \sum_j X_j K_{ij} \tag{14}$$

8

where X_j is the mole fraction of species j for a gas mixture of reservoir number density n_{T_0}. The Mach number of the flow field is M, and γ is the specific heat ratio for the mixture. Further, the mixture gram molecular weight $<\overline{M}>$ is given by

$$<\overline{M}> = \sum_i \overline{M}_i X_i \tag{15}$$

From Eq. (14) it is seen that the average number of collisions Z_i (x_2, x_1) experienced by a molecule of species i over spatial interval $(\hat{x}_2, \hat{x}_1)$, $\hat{x}_2 > \hat{x}_1$, is given by

$$Z_i(\hat{x}_2,\hat{x}_1) = \int dZ_i = n_{T_0}D[<\overline{M}>/\gamma RT_0]^{1/2} \cdot \sum_j X_j \int_{\hat{x}_2}^{\hat{x}_2} d\hat{x} \cdot F^{(\gamma-3)/2(\gamma-1)} \cdot K_{ij} \tag{16a}$$

where

$$F = 1 + [(\gamma - 1)/2] M^2$$

The evaluation of Eq. (16a) clearly requires specification of the rate coefficient, K_{ij}, and the relationship of the Mach number, M, and the axial position, $\hat{x}$. For a conical nozzle of expansion half-angle θ, it can be shown that

$$\hat{x} \tan \theta = -1 + [2/(\gamma + 1)]^{(\gamma + 1)/4(\gamma - 1)} \cdot (1/\sqrt{M}) \cdot F^{(\gamma + 1)/4(\gamma - 1)} \tag{16b}$$

2.3 EVALUATION OF RATE COEFFICIENT AND COLLISION NUMBER FOR SELECTED POTENTIAL FUNCTIONS

The rate coefficient K(T) is evaluated initially for the class of single-term, attractive intermolecular potentials which vary inversely with the distance of separation of the colliding species, i.e.,

$$\phi(r) = -\bar{a}/r^s , s > 0 \tag{17}$$

where $\bar{a}$ denotes the strength of the interaction. It will be seen that closed-form expressions are obtained for $\sigma(v)$ for this class of potential function.

The essence of the cross-section calculation is the specification of those processes which lead to close molecular encounters. Such close encounters occur continuously, of course, if the species are bound and orbiting one another; or if, for a given impact parameter (b), the collision energy is sufficiently great to surmount the centrifugal barrier; or, thirdly, if, for a given energy, the impact parameter is sufficiently small that collisions occur (Refs. 1, 2, and 3). It is this close encounter of the third kind which is of interest.

9

Figure 1 shows the radial variation of the effective potential $\phi_{eff}(r)$ for a potential $\phi(r) = \bar{a}/r^s$ where $\phi_{eff}(r)$ is defined to be the sum of $\phi(r)$ and the centrifugal potential (Ref. 2)

$$\phi_{eff}(r) = \phi(r) + (\bar{m}v_0^2 b^2/2r^2) \tag{18}$$

The initial speed and impact parameter are v_0 and b, respectively. Defining r^* by

$$[d\phi_{eff}(r)/dr]_{r = r^*} = 0 \tag{19}$$

one finds the maximum height $\phi_{eff}(r^*)$ of the centrifugal barrier to be

$$\phi_{eff}(r^*) = [(\bar{m} v_0 b^2)^{s/(s-2)}/(\bar{a}s)^{2/(s-2)}][(1/2) - (1/s)] \tag{20}$$

From Eq. (20) it is seen that, for a given initial energy and speed v_0, the height of the centrifugal barrier increases as $b^{2s/(s-2)}$. As shown in Fig. 1, if $\bar{m} v_0^2/2 = E < \phi_{eff}(r^*)$, the interaction occurs at large values of r which, in general, is ineffective for energy transfer processes. If, however, $E > \phi_{eff}(r^*)$, penetration and a close encounter occurs, satisfying the normal prerequisite for an inelastic process.

Regarding E as constant, the critical impact parameter b_c is given by

$$E = \phi_{eff}(r^*) \tag{21a}$$

so that

$$b_c^2 = (\bar{a}s/E)^{2/s}[(s-2)/s]^{(2-s)/s} = (as/\bar{m} v_0^2)^{2/s} [(s-2)/s]^{(2-s)/2} \tag{21b}$$

Consequently, if $b < b_c$, $E > \phi_{eff}(r^*)$ and a close encounter occurs; $b > b_c$, $E < \phi_{eff}(r^*)$, and the collision turning point exceeds r^*, which defines a collision which is generally ineffective for energy transfer processes. The collision cross section σ is defined, therefore, to be

$$\sigma = \pi b_c^2 = \pi(\bar{a}s/\bar{m} v_0^2)^{2/s} [s/(s-2)]^{(s-2)/s} \tag{22}$$

which shows σ to be a function of speed. The evaluation of the rate coefficient $K(T)$ follows immediately (Ref. 2)

$$K(T) = \bar{a}^{2/s} (\pi/\bar{m})^{1/2} \cdot 2^{(3s-4)/2s} \cdot (s-2)^{2/s} (k_B T)^{(s-4)/2s} \Gamma[(s-2)/s] \tag{23}$$

10

where $\Gamma(x)$ denotes the gamma function of x.

Using Eq. (23) for the rate coefficient K(T) for attractive inverse power law potentials in Eq. (16), it is seen that, for isentropic expansions, the cumulative collision number $Z_{ij}(\hat{x},\hat{x}_1)$ is given by

$$Z_{ij}(\hat{x},\hat{x}_1) = \xi_{ij} \cdot n_{To} \cdot D\left[\frac{<\overline{M}>}{M_{ij}}\right]^{\frac{1}{2}} \cdot \left(\frac{\pi}{\gamma}\right)^{\frac{1}{2}} \cdot \alpha_s \cdot \overline{a}^{2/s} \cdot (k_BT_o)^{-2/s} \cdot X_j \cdot \int_{\hat{x}_1}^{\hat{x}} (1/M) \, Fd\hat{x}'$$

(24)

where $Z_{ij}(\hat{x},\hat{x}_1)$ represents the average number of collisions experienced over the $(\hat{x},\hat{x}_1)$ interval by an ith species molecule with j-species molecules.

Further,

$$\overline{M}_{ij} = N_A \overline{m}_{ij}$$

and

$$\alpha_s = 2^{(3s-4)/2s}(s-2)^{2/s} \cdot \Gamma[(s-2)/s]$$

Clearly, the total cumulative collision number $Z_i(\hat{x},\hat{x}_1)$ regardless of the species of collision partner is given by

$$Z_i(\hat{x}, \hat{x}_1) = \sum_j Z_{ij}(\hat{x}, \hat{x}_1)$$

(25)

where the summation over "j" includes the index "i".

Equation (24) is generalized easily to include those cases for which the potential index "s" varies with the jth species; i.e., $s = s_{ij}$. Specifically, if

$$\phi_{ij}(r) = -\overline{a}_{ij}/r^{s_{ij}}$$

Eq. (24) is made more general by adding the "ij" subscript pair to the parameters s and $\overline{a}$.

Further simplification of appearance of Eq. (24) results by defining the interaction parameter $\overline{a}_{ij}$ to be the product of a characteristic energy ϵ_{ij} and a characteristic range parameter $\overline{d}_{ij}$, i.e.,

$$\phi_{ij}(r) = -\epsilon_{ij}(\overline{d}_{ij}/r)^{s_{ij}}$$

11

so that

$$\bar{a}_{ij} = \epsilon_{ij} (\bar{d}_{ij})^{s_{ij}}$$

Using these characteristic parameters the dimensionless temperature, (T^*), throat diameter (D^*), and number density (n^*) are defined as

$$T^*_{ij} = T/(\epsilon_{ij}/k_B)$$

$$D^*_{ij} = D/\bar{d}_{ij}$$

and

$$n^*_{ij} = n(\bar{d}_{ij})^3$$

Equation (24) can now be written as

$$\bar{Z}(\hat{x},\hat{x}_1) = Z(\hat{x},\hat{x}_1)/\{\xi \cdot \alpha_s \cdot \sqrt{\pi} \cdot n^*_{T_0}D^*(T^*_0)^{-2/s}[<\overline{M}>/\overline{M}_{ij}]^{\frac{1}{2}} X_j\} \qquad (26a)$$

$$= (1/\gamma)^{\frac{1}{2}} \cdot \int_{\hat{x}_1}^{\hat{x}} (1/M)F^{-[(1/\gamma-1)-(2/s)]} d\hat{x}' \qquad (26b)$$

The explicit use of the subscript pair "ij" has been suppressed when requirements for its use are obvious.

The total cumulative collision number $Z_i(\hat{x},\hat{x}_1)$ for a gas mixture is given by

$$Z_i(\hat{x},\hat{x}_1) = \sum_j Z_{ij}(\hat{x},\hat{x}_1) = (\pi/\gamma)^{\frac{1}{2}} \cdot \sum_j \xi_{ij} \alpha_{s_{ij}} (n^*_{T_0}D^*)_{ij}(T^*_0)_{ij}^{-2/s_{ij}}[<\overline{M}>/\overline{M}_{ij}]^{\frac{1}{2}}x_j$$

$$\cdot \int_{\hat{x}_1}^{\hat{x}} (1/M)F^{-[1/(\gamma-1)-(2/s_{ij})]}dx' \qquad (26c)$$

where

$$T^*_0 = T_0/\epsilon_{ij}$$

$$(n^*_{T_0} D)_{ij} = n_{T_0} D \bar{d}^2_{ij}$$

and

$$\phi_{ij} = -\epsilon_{ij}(d_{ij}/r_{ij})^{s_{ij}}$$

To obtain comparable results for the hard-sphere interaction cumulative collision number, Z^{HS}_{ij}, one may, of course, use Eqs. (9) and (16) or quite simply take the limit of Eq. (24) as the parameter s approaches ∞. The result is found to be

$$\bar{Z}^{HS}_{ij} = \bar{Z}^{HS}_{ij}/\{\xi \, 2^{3/2}(\pi)^{\frac{1}{2}} \cdot n^*_{T_0}D^*[<\overline{M}>/\overline{M}_{ij}]^{\frac{1}{2}}X_j\} \qquad (27a)$$

$$= (1/\gamma)^{\frac{1}{2}} \cdot \int_{\hat{x}_1}^{\hat{x}} (1/M) \cdot F^{-1/(\gamma-1)} d\hat{x}'$$ (27b)

The hard-sphere characteristic distance d_{ij} is defined by

$$d_{ij} = (d_i + d_j)/2$$

From Eq. (27a) it is seen that $\bar{Z}_{ij}^{HS}(\hat{x}, \hat{x}_1)$ is independent of the reservoir temperature T_0.

For gas mixtures the total collision number $\bar{Z}_i^{HS}$ is defined in a manner similar to that of Eq. (26c).

The variation of collision number $\bar{Z}_{ij}$ with the nozzle expansion angle is most clearly seen by transforming the independent variable of the previous equations from axial position $\hat{x}$ to Mach number M. As an example, using Eq. (26b) one finds

$$\bar{Z}(M, M_1) = (\cot \theta/4) g(\gamma) \int_{M_1}^{M} dM \left[\frac{M^2 - 1}{M^{5/2}} \right] \cdot F^{(2/s) \cdot [(3\gamma - 1)]/[4(\gamma - 1)]}$$ (27c)

where

$$g(\gamma) = (1/\gamma)^{\frac{1}{2}} [2/(\gamma + 1)]^{(\gamma + 1)/4(\gamma - 1)}$$

From Eq. (27c) it is seen that the nondimensional collision number $\bar{Z}(M, M_1)$ varies, or scales, according to $\cot \theta$, a result which is well-known. Further, the Mach number M and axial distance x are related by the usual Mach number-expansion area relationship for isentropic conical nozzle expansions or M versus x relations provided by method of characteristics solutions for external, vacuum-expansion flow fields.

The motivation for using single-term potentials of the form $\phi(r) = -\bar{a}/r^s$ has been noted to be, rather than accuracy, the ability to obtain closed-form expressions for the rate coefficient K (T) and simple scaling laws for the collision numbers. To improve the accuracy of the description of the intermolecular interaction, it is known that intermolecular potentials of two or more terms are required. For nonpolar interactions a reasonably successful potential is the Lennard-Jones 12:6 potential:

$$\phi(r) = 4\epsilon[(\bar{d}/r)^{12} - (\bar{d}/r)^6]$$ (28)

where the range parameter d, the molecular diameter, is the intermolecular separation distance at which ϕ is zero and ϵ, the characteristic strength parameter, is the well-depth of

the interaction. For this interaction $\phi(r)$ it is known that, to first-order, the viscosity, $[\eta]_1$, of a pure gas (Ref. 1) is given by

$$[\eta]_1 = (5/16)\ (\pi m k_B T)^{1/2}/\pi \overline{d}^{\ 2}\ \Omega^{(2,2)*}(T) \tag{29}$$

where $\Omega^{(2,2)*}(T^*)$ is the collision integral $\Omega^{(k,s)*}(T^*)$ for $\ell = s = \pm 2$ and $T^* = T/(\epsilon/k_b)$.

For the hard-sphere interaction

$$\eta^{HS} = (5/16)\ (\pi m k_B T)^{1/2}/\pi d^2 \tag{30}$$

so that comparison of Eqs. (29) and (30) shows that the previous results for the collision numbers for the hard-sphere interaction can be modified to describe the 12:6 $\phi(r)$ interaction by replacing the hard-sphere parameter d^2 with the 12:6 product of parameters $\overline{d}^2\Omega^{(2,2)*}(T^*)$. Therefore, for the 12:6 interaction, recalling Eq. (11),

$$K(T^*) = (\epsilon/k)^{1/2} \cdot \overline{d}^2\ \Omega^{(2,2)}(T^*) \cdot [4\pi RT^*/\overline{M}\ ]^{1/2} \tag{31}$$

Now, from Eqs. (27a) and (27b),

$$\overline{Z}_{ij}^{12:6}\ (\hat{x},\hat{x}_1) = Z_{ij}^{12:6}(\hat{x},\hat{x}_1)\ /\ \{\xi \cdot 2^{3/2} \cdot \pi^{1/2}\ n_{T_0}^* \cdot D^*[<\overline{M}>/\overline{M}_{ij}]^{1/2} \cdot X_j\} \tag{32a}$$

$$= (1/\gamma)^{1/2} \cdot \int_{\hat{x}_i}^{\hat{x}}(1/M)\ \Omega_{ij}^{(2,2)*}\ (T_o^*/F) \cdot F^{-1/(\gamma - 1)}\ d\hat{x}' \tag{32b}$$

where $\Omega_{ij}^{(2,2)*}$ is the reduced collision integral for binary mixtures (Ref. 1).

For "i-j" species interactions

$$\overline{d}_{ij} = (\overline{d}_i + \overline{d}_j)/2$$

and

$$\epsilon_{ij} = (\epsilon_i \epsilon_j)^{1/2}$$

Consequently, the total cumulative collision number $\overline{Z}_i^{12:6}(\hat{x},\hat{x}_1)$ is given by

$$\overline{Z}_i^{12:6}(\hat{x},\hat{x}_1) = \Sigma_j\ \overline{Z}_{ij}^{12:6}\ (\hat{x},\hat{x}_1) \tag{33a}$$

$$= (8\pi/\gamma)^{1/2} \cdot \underset{j}{\Sigma}\ \xi_{ij}(n_{T_0}^*D^*)_{ij}[<\overline{M}>/\overline{M}_{ij}]^{1/2} \cdot X_j \cdot \int_{\hat{x}_1}^{\hat{x}} d\hat{x}'\ (1/M)\ \Omega_{ij}^{(2,2)*}\ (T_o^*/F) \cdot F^{-1/(\gamma - 1)}$$

where the nondimensional reservoir parameters n_{To}^* and T_o^* are defined by

$$\left(n_{To}^* D^*\right)_{ij} = \left(n_{To} \cdot D\right)\bar{d}_{ij}^2 \tag{33b}$$

and

$$\left(T_o^*\right)_{ij} = T_o/(\epsilon_{ij}/k_B) \tag{33c}$$

From Eqs. (32) and (33) it is seen that, unlike the simple inverse $-r^s$ potentials, the collision number integral does not exhibit simple multiplicative scaling with T_o^*.

For a single, gaseous, polar species of dipole moment μ, the appropriate potential function is the Stockmayer potential (Ref. 1):

$$\phi(r) = 4\epsilon\left[(\bar{d}/r)^{12} - (\bar{d}/r)^6\right] - (\mu^2/r^3)\, g\left(\bar{\theta}_1,\theta_2,\bar{\phi}_2 - \phi_1\right) \tag{34a}$$

where $(\bar{\theta}_i, \bar{\Phi}_i)$ are the spherical polar and aximuthal angles, respectively, of alignment of the dipole moments of the molecules. Further, it can be shown (Ref. 1) that

$$g(\bar{\theta}_1,\bar{\theta}_2,\bar{\phi}_2 - \bar{\phi}_1) = 2\cos\bar{\theta}_1\cos\bar{\theta}_2 - \sin\bar{\theta}_1\sin\bar{\theta}_2\cos(\bar{\phi}_2 - \bar{\phi}_1)$$

Monchick and Mason (Ref. 4) have calculated various $\Omega^{(k,s)*}$ functions for the Stockmayer potential, but only after replacing the angle-dependent potential by a central potential. The procedure for this computation is given in Ref. 4 and, in short, consists of the computation of the collision cross section for a fixed orientation and the thermal averaging of the resulting cross sections over the range of potentials which can occur in a collision. The values of $\Omega^{(2,2)*}$ for such a thermally averaged Stockmayer potential are given in Ref. 4 for the reduced temperature range $0.1 \leq T^* \leq 100$ and for the range of δ^*

$$0 \leq \delta^* \leq 2.5$$

where

$$\delta^* = (1/2)[\mu^2/(\epsilon\bar{d})^3] \tag{34b}$$

It should be noted that for $\delta^* = 0$, $\Phi(r)$ becomes the Lennard-Jones 12:6 potential and, as a result, values of $\Omega^{(l,s)*}$ for the 12:6 potential are given in Refs. 1 and 4 for $0.1 \leq T^* \leq 100$.

To appreciate the limitations imposed by a minimum T^* of 0.1 for the collision integral tables, it is seen from the data of Ref. 1 for the well-depths of various molecular species that the existing $\Omega^{(l,s)*}$ tables are inadequate for flow-field calculations for CO_2 for $T \leq 20$ K and for both organic and halogen species for $T \leq 50$ K. A similar situation exists for polar

species for which well-depths ϵ/k may be approximately 400 K, thereby yielding a minimum T for flow-field calculations of approximately 40 K. In other terms, for $\gamma = 1.2$, $T^* = 0.1$ corresponds to a free-stream Mach number of approximately 9.5 above which collision integral-based calculations are impossible with the existing tables of the previously quoted references.

To remedy this deficiency it was necessary to compute values of $\Omega^{(2,2)^*}$ for $T^* \leq 0.1$ for both nonpolar and polar species. To accomplish this a computer program was acquired from the Computer Program Library of Queen's University of Belfast, Northern Ireland. This program, developed by O'Hara and Smith (Ref. 5), computes $\Omega^{(l,s)^*}(T^*)$ for specified accuracy for $l,s \leq 6$ over a specified range of T^* for interaction potentials $\phi(r)$ which go to zero faster than r^{-2} as $r \rightarrow \infty$. Using the program of O'Hara and Smith, $\Omega^{(l,s)^*}(T^*)$ values were computed for the 12:6 potential for the range $0.01 \leq T^* \leq 1.1$, and good agreement was obtained with the published values of Refs. 1 and 4 for $T^* \geq 0.1$.

The Stockmayer potential of Eq. (34) presented additional problems, for it was believed to be too time-consuming and unwarranted for this work to perform the potential function-averaging as was done by Monchick and Mason. A more simplistic approach was taken. The Stockmayer potential was replaced by the Krieger central-field potential

$$
\begin{aligned}
\phi(r) &= 4\epsilon[(\bar{d}/r)^{12} - (\bar{d}/r)^6] + \zeta(2\mu^2/r^3) \\
&= 4\epsilon[(\bar{r})^{-12} - (\bar{r})^{-6}] + \zeta\delta^* \cdot (\bar{r})^{-3}
\end{aligned}
\tag{35}
$$

where ζ is $+1$ and -1 for parallel and anti-parallel alignment, respectively, of the dipole moment vectors $(\vec{\mu})$ and $\bar{r} = \bar{d}/r$.

Clearly, for high temperatures, the dipole-dipole interaction term will diminish in importance and the 12:6 $\phi(r)$ results will be obtained. Values of $\Omega^{(2,2)^*}(T^*)$ were calculated for $\zeta = \pm 1$, and Table 1 shows the results for $0.01 \leq T^* \leq 30$. Also shown in Table 1 are the results, $\Omega^{(2,2)^*}_{MM}$ of Ref. 6 for the potential-averaged cases, and the large differences are noted. Denoting $\Omega^{(2,2)^*}_\zeta(T^*)$ to be the collision integral for specified ζ, the geometric mean $\Omega^{(2,2)^*}_{gm}(T^*)$ of the two values of $\Omega^{(2,2)^*}_\zeta(T^*)$ was calculated; i.e.,

$$
\Omega^{(2,2^*)}_{gm}(T^*) = [\Omega^{(2,2)^*}_{+1}(T^*) \cdot \Omega^{(2,2)^*}_{-1}(T^*)]^{1/2}
$$

The values shown in Table 1 were determined for $\zeta^* = 0.25$ which, although arbitrarily selected, coincides with one of the values presented in Ref. 6.

For $T^* \geq 0.1$ the integrated collision numbers were determined using $\Omega^{(2,2)^*}(T^*)$ obtained from Ref. 6, $\Omega_{\pm 1}^{(2,2)^*}(T^*)$ and $\Omega_{gm}^{(2,2)^*}(T^*)$, all for the value of $\delta^* = 0.25$. For $0.01 \leq T^* \leq 0.1$, obviously, only the last three collision integrals could be used. From Table 1 it is seen that $\Omega_{gm}^{(2,2)^*}$ closely approximates $\Omega_{MM}^{(2,2)^*}$ for $T^* \geq 0.1$, and, specifically $0.90 \leq \Omega_{MM}^{(2,2)^*}/\Omega_{gm}^{(2,2)^*} \leq 1.04$ over the range of $0.1 \leq T^* \leq 30$. Consequently, the suggested approach for the determination of $\Omega^{(2,2)^*}$ for polar species is not to use the rather gross and nonmonotonic interpolation in δ^* required by use of the results of Ref. 6, but rather, if available, to employ the calculation of Ref. 5 from which $\Omega_{gm}^{(2,2)^*}(T)^*$ can be obtained for any specific value of δ^* desired. The extrapolation of $\Omega_{gm}^{(2,2)^*}$ to the region $T^* \leq 0.1$ cannot be rigorously justified but is used for lack of anything better and its demonstrated accuracy at higher temperatures. Finally, generalization of the equations involving the collision integrals $\Omega^{(2,2)^*}(T^*)$ to mixtures of both nonpolar and polar gases is straightforward and described in detail in Refs. 1 and 7.

3.0 RESULTS AND DISCUSSION

3.1 HARD-SPHERE AND INVERSE -r^s POTENTIALS

The preceding formulation was used to determine the cumulative nondimensional collision number $\overline{Z}(\hat{x}_2, \hat{x}_1)$ for conical nozzle expansion flow fields. Of particular interest were the variations in $\overline{Z}(\hat{x}_2, \hat{x}_1)$ with nozzle expansion half-angle, reservoir properties, and the type of interaction potential which was assumed for the intermolecular collisions. To coincide with previous work, Refs. 8, 9, and 10, the nozzle expansion half-angles $\theta = 5$, 10.5, and 15 deg were studied, and the axial range investigated was $o \leq \hat{x} \leq 25$, where $\hat{x}$ was measured with respect to the nozzle throat. For reference, Figs. 2, 3, and 4, respectively, show the axial variations for M, $\overline{T} = T_\infty/T_0$, and $\overline{n} = n_\infty/n_0$ for these half-angles for the specific heat ratios $\gamma = 5/3$, 7/5, and 9/7. As Eq. (16b) shows, M is a function of $\hat{x} \tan \theta$ as are $\overline{T}$ and $\overline{n}$. Therefore, the independent variable in Figs. 2 through 4 is $\hat{x} \tan \theta$ which allows evaluation for any desired expansion angle.

The intermolecular interaction potentials studied included the hard-sphere, inverse -r^s for s = 3 and 6, the two-term Lennard-Jones 12:6 potential, and the averaged three-term Stockmayer and the Krieger potentials. The collision number $\overline{Z}(\hat{x},o)$ was calculated by numerical integration of Eq. (27b) for the T_o-independent hard-sphere interaction and by integration of Eq. (27a) for the interactions

$$\phi_3(r) = -\overline{a}_3/r^3$$

and

$$\phi_6(r) = -\overline{a}_6/r^6$$

From Eq. (26a) for the inverse $-r^s$ potential

$$\phi_s(r) = -\bar{a}_s/r^s$$

it is seen that $\overline{Z}(\hat{x}_2,\hat{x}_1)$ varies with the reservoir number density and throat diameter as $n_{To}^* D$, which is to be expected for the binary collision model. Obviously, an identical result is obtained for all potentials in this work. Further, from Eq. (26a) it is seen that $\overline{Z}(\hat{x}_2,\hat{x}_1)$ varies with the resevoir temperature as $T_o^{-2/s}$. Figure 5 shows the variation with T_o of the ratio of the collision numbers $\overline{Z}(\hat{x}_2,\hat{x}_1)_{T_o = 300 K}/\overline{Z}(\hat{x}_2,\hat{x}_1)_{T_o}$ at the reservoir temperatures of 300 K and T_o. This variation is shown for the interaction potential parameter s values of 3, 4, 6, and 8, which correspond, respectively, to dipole-dipole, charge-induced dipole, induced dipole-induced dipole, and induced dipole-induced quadrupole molecular interactions. From Fig. 5 it is seen that for the T_o range of 50 to 2000 K the collision ratio dependence on T_o varies from an approximate factor of 10 for $s = 3$ to an approximate factor of 3 for $s = 8$. Clearly, the longer the interaction range (the smaller the s value), the greater the temperature variation of the collision number $\overline{Z}(\hat{x}_2,\hat{x}_1)$.

Figures 6a, b, and c show the variation of the hard-sphere interaction cumulative collision number $\overline{Z}_{ij}^{HS}(\hat{x},o)$ with axial distance $\hat{x}$ for $\gamma = 5/3$, 7/5, and 9/7, respectively, for the expansion half-angles of $\theta = 5$, 10.5, and 15 deg. Included as additional abscissae for all figures for $\overline{Z}(x,o)$ versus $\hat{x}$ are the corresponding Mach numbers for the half-angles $\theta = 5$, 10.5, and 15 deg. Shown in Fig. 6a for illustrative purposes are the loci for the constant integer Mach numbers of 2 through 7 for $\gamma = 5/3$. Figures 7a, b, and c show the variation with $\hat{x}$ of the cumulative fraction of collisions for these same cases, and it is seen that at $\hat{x} = 10$ for $\theta = 5$, 10.5, and 15 deg approximately 90 percent of the collisions have occurred. Figures 8a, b, and c and 9a, b, and c show similar results for the variation of $\overline{Z}_{ij}(\hat{x},o)$ for the inverse $-r^3$ and inverse $-r^6$ potentials, respectively.

If $M(w\%)$ is defined to be the Mach number at which w percent of the collisions occur for a given intermolecular potential interaction and expansion γ, Figs. 10a, b, and c show the variation with γ of $M(50\%)$, $M(90\%)$ and $M(99\%)$ for the hard-sphere, r^{-6}, and r^{-3} potentials, respectively. From Eq. (27c) it is seen that these results are independent of θ, and Fig. 2 yields the axial positions corresponding to these Mach numbers for the specified γ and θ values. Figure 10a shows that for the hard-sphere interaction 50 percent of the total collisions in the expansion occur at $M \doteq 2$, and this result is independent of γ for the range of γ investigated. Figure 10b shows that for the inverse $-r^6$ interaction the result is nearly identical. For the long-range, inverse $-r^3$ potential, $M(50\%)$ is approximately 2.5 and independent of γ to within ± 10 percent. Clearly, increasingly greater variation with γ occurs for $M(w\%)$ as w increases. Shown in Fig. 11 is the variation of $\overline{Z}_{ij}(25.5,0)$ with expansion half-angle θ, and the results for the r^{-3}, r^{-6}, and hard-sphere potentials are shown for the γ

values of 5/3, 7/5, 9/7. From these results it is seen that for a conical nozzle of fixed expansion length $\hat{x} = 25.5$ the collision number $\overline{Z}_{ij}(25.5,0)$ decreases with increasing θ from 5 to 15 deg by an approximate factor of 3 regardless of the specific heat ratio γ and interaction potential. Further, for a specified θ, the variation of $\overline{Z}(25.5,0)$ with type of potential interaction is, again, approximately a factor of 1.5 to 2 increase from the short-range hard-sphere results to those of the longer range inverse -r^3 values. It should be noted in Fig. 10 that the collision number $\overline{Z}(25.5,0)$ for the inverse -r^6 interaction is quite insensitive to variations in the specific heat ratio, γ. Specifically, for all three nozzle angles used, there is approximately only a six percent variation in $\overline{Z}(25.5,0)$ for the range of γ shown in Fig. 11. Similar conclusions apply to axial values other than $\hat{x} = 25.5$. This insensitivity of $\overline{Z}_{ij}$ to γ is of particular interest for experimental studies of spectral line-broadening phenomena of molecular species for which the long-range r^6 term is dominant for the phase-interrupting collisions. For such species, Fig. 10 shows that the effect of molecular relaxation and the resulting γ change are of little importance in the calculation of $\overline{Z}(\hat{x}_2,\hat{x}_1)$. Further, for the range 5 deg $\leq \theta \leq$ 15 deg estimates of $\overline{Z}(\hat{x},o)$ for either the r^3 or r^6 interactions can be obtained by using the hard-sphere results for any θ within this range, and the resulting estimate will be incorrect by less than a factor of 10. Conversion of the nondimensional $\overline{Z}(\hat{x},o)$ results to the actual collision number is effected easily by use of the appropriate scaling constants given in the previous equations.

3.2 LENNARD-JONES 12:6, STOCKMAYER AND KRIEGER POTENTIAL RESULTS

Since simple multiplicative scaling in T_o^* is not possible for the $\overline{Z}(\hat{x},o)$ results for the two- and three-term potentials, computations were found for the T_o^* values of 2, 5, and 10, which for typical nonpolar species correspond approximately to the T_o range of 200 to 400 K up to 2000 to 4000 K. For polar species the lower and upper limits of the T_o range are increased by a nominal factor of 2.

The γ values used previously were employed, but only $\theta = 5$ deg was used for the calculation. Scaling to other expansion angles has been described previously and can be performed to obtain results for values of θ other than 5 deg. Figures 12a, b, and c show the axial distance and Mach number variations of $\overline{Z}(\hat{x},o)$ for $\gamma = 5/3$, 7/5, and 9/7, respectively, for the Lennard-Jones 12:6 potential. The variation of $\overline{Z}_{ij}(\infty,o)$ with T_o^* over the T_o^* over the T_o^* range 2 to 10 is shown in Fig. 13 for $\gamma = 5/3$, 7/5, and 9/7. From these results it is seen that $\overline{Z}_{ij}(\infty,o)$ varies inversely with T_o^* as expected; i.e., for large T_o^* values the average collision energy will be sufficiently great so that the attractive portion of the potential will have but little effect. However, as T_o^* decreases the term -$4\epsilon(\overline{r})^{-6}$ assumes greater importance, and the results will resemble more nearly those for the inverse -r^6 potential results.

It is interesting to compare directly the distance and Mach number variations of the collision number with T_o^* for the hard-sphere, inverse -r^6, and 12:6 potentials. Comparison

of the last two potentials will indicate, as a function of T_0^*, the degree of inaccuracy of using the easily scaled, inverse $-r^6$ potential function. Further, comparison of the 12:6 and hard-sphere potentials will show that the hard-sphere collision diameter will be temperature-, or T_0^*-, dependent; and knowledge of this dependence will enable correction of previous collision number calculations based on hard-sphere potential interactions (Ref. 11). To make such a comparison it is necessary to ensure that the same $\overline{Z}(\hat{x},o)$ function is being used, for, when possible, T_0^* has been eliminated from the integrated collision number. If this common integrated collision number is defined to be $\tilde{Z}(\hat{x},o)$ and the 12:6 $\overline{Z}(\hat{x},o)$ functional form is chosen for reference,

$$\tilde{Z}_{ij}^{12:6}(\hat{x},o) \equiv \overline{Z}_{ij}^{12:6}(\hat{x},o) = Z_{ij}^{12:6}(\hat{x},o)/\{\xi \cdot 2^{3/2} \cdot \pi^{\frac{1}{2}} \cdot r_{T_0}^* D^*[<\overline{M}>/M_{ij}]^{\frac{1}{2}} X_j\} \quad (36)$$

For the hard-sphere case, Eqs. (27a) and (27b) show that

$$\tilde{Z}_{ij}^{HS}(\hat{x},o) = (\overline{\overline{d}}_{ij}/\overline{d}_{ij})^2 \cdot \overline{Z}_{ij}^{HS}(\hat{x},o) \quad (37)$$

where $\overline{\overline{d}}_{ij}$ is the hard-sphere diameter which is acknowledged to be unequal to $\overline{d}_{ij}$; i.e., if the characteristic lengths are determined from either second virial coefficient data or viscosity measurements, the resulting value of d_{ij} will depend upon the assumed form of the interaction potential. To transform the inverse $-r^s$ potential collision number, Eqs. (26a) and (26b) show that

$$\tilde{Z}_{ij}^{(s)}(\hat{x},o) = (\alpha_s/2^{3/2})(T_0^*)^{-2/s} \cdot \overline{Z}_{ij}^{(s)}(\hat{x},o) \quad (38)$$

where, again,

$$\alpha_s = 2^{(3s-4)/2s} \cdot (s-2)^{s/2} \cdot \Gamma[(s-2)/s]$$

For $s = 6$,

$$(\alpha_6/2^{3/2})(T_0^*)^{-2/s} = 1.7062 \ (T_0^*)^{-1/3}$$

Therefore,

$$\tilde{Z}_{ij}^{(6)}(x,o) = 1.7062 \ (T_0^*)^{-1/3} \ \overline{Z}_{ij}^{(6)}(\hat{x},o) \quad (39)$$

Figures 14a, b, and c show the variation with T_0^* of $\tilde{Z}_{ij}(\infty,o)$ for the three potential functions for $\gamma = 5/3, 7/5$, and $9/7$. For all three values of γ, it is seen that for the lowest T_0^* (= 2) flow-field expansions, the 12:6 results are approximately a factor of 2 larger than the

hard-sphere results. Further, this difference decreases as T_o^* increases, which is to be expected, for, as T_o^* increases, the average intermolecular collision energy increases and the importance of the dispersion energy term in the 12:6 potential lessens. The penetration distance of separation decreases with increasing T_o^*, and the 12:6 results equal the hard-sphere results at a value of T_o^* which depends upon γ, or the expansion characteristics, or history. Clearly, $\widetilde{Z}^{12:6}(\infty,o) < \widetilde{Z}^{HS}(\infty,o)$, assuming $\overline{\overline{d}}_{ij} = \overline{d}_{ij}$, which shows that the average distance of closest approach is less than $\overline{d}_{ij}$.

It is seen from Figs. 14a, b, and c that the results of the inverse $-r^6$ potential differ from those of the 12:6 potential by less than 20 percent over the investigated ranges T_o^* and γ, which, for certain applications, is a sufficiently small difference to recommend the use of the more easily scaled inverse $-r^6$ potential interaction.

Finally, using the results of Figs. 14a, b, and c and Eq. (37), the ratio $\overline{\overline{d}}_{ij}/\overline{d}_{ij}$ was determined as a function of T_o^*. Figure 15 shows these results for $\gamma = 5/3, 7/5$, and $9/7$ for both $\overline{Z}_{ij}^{(6)}(\infty,o)$ and $\overline{Z}_{ij}^{12:6}(\infty,o)$; i.e., the ratio $\overline{\overline{d}}_{ij}/\overline{d}_{ij}$ was determined to yield equal values of the just-mentioned collision numbers and $\widetilde{Z}^{HS}(\infty,o)$. The strong T_o^* dependence and the much weaker variation with γ of the $\overline{\overline{d}}_{ij}/\overline{d}_{ij}$ ratio are evident in Fig. 14, and these results should be useful for making corrections to hard-sphere elastic collision number calculations to obtain the more accurate 12:6 potential results.

The difficulties associated with the calculation of the collision number $Z_{ij}^{12:6:3}(\hat{x}_2,\hat{x}_1)$ for the Stockmayer potential have been discussed previously. Shown in Fig. 16 is the variation of $\overline{Z}_{ij}^{12:6:3}(\hat{x},o)$ with the axial distance parameter $\hat{x} \tan \theta$ and Mach number M. The results shown in Fig. 16 were obtained for $\gamma = 5/3$, $T_o^* = 5$, and $\delta^* = 0.25$ and are presented to exemplify the differences obtained using the various and previously described collision integrals $\Omega^{(2,2)*}(T^*, \delta^*)$. Note that the results obtained using the $\Omega^{(2,2)*}$ values of Monchick and Mason are in excellent agreement with the $\Omega^{(2,2)*}$ values which are the geometric mean of those obtained for $\zeta = \pm 1$ of Eq. (35). Additionally, $\overline{Z}_{ij}^{12:6:3}(\hat{x},o)$ obtained using $\zeta = \pm 1$ differ from the Monchick-Mason and geometric mean values by approximately ± 20 percent, respectively; greater differences are to be expected for $\delta^* > 0.25$.

4.0 SUMMARY AND CONCLUSIONS

The cumulative elastic collision number of molecules has been calculated for the supersonic region of isentropic, continuum conical nozzle flow fields for gaseous species characterized by the specific heat ratios $\gamma = 5/3, 7/5$, and $9/7$. The cumulative collision number was determined as a function of Mach number and axial distance parameter $\hat{x} \tan \theta$, the latter of which was specialized to the nozzle half-angles $\theta = 5, 10.5$, and 15 deg. The calculations were extended to study the effects of the type of intermolecular potential

interaction on the cumulative collision number. Specifically, the interaction potentials investigated included the attractive inverse $-r^3$ and inverse $-r^6$ potentials; the Lennard-Jones 12:6; the Stockmayer and Krieger 12:6:3 potentials; and the hard-sphere interaction. The results have been presented in nondimensional form in terms of the characteristic well-depth energies and ranges of the intermolecular potentials, and the range of the nondimensional reservoir temperature studied was $2 < T_o^* < 10$, which corresponds to the range of approximately 200 to 1000 K for typical nonpolar molecular species.

For the inverse $-r^3$ potentials a close encounter collision model was employed for calculation of the elastic collision cross section which resulted in simple multiplicative scaling of the nondimensional collision number with reservoir temperature. However, for the two- and three-term potentials it was necessary to perform the calculations using the kinetic theory collision integrals $\Omega^{(2,2)*}(T^*)$. For these cases it was necessary to extend the lower range of the temperature of the published collision integral tables from $T^* = 0.1$ to $T^* = 0.01$ to cover the required Mach number range of the flow field. Special problems were encountered in this extension with the 12:6:3 potential, and the extended tabular data for this case are used without rigorous justification.

The results for the nondimensional cumulative number have been generalized to describe gaseous mixtures, and detailed comparisons of the hard-sphere, inverse $-r^6$, and the Lennard-Jones potentials were presented. The collision number for the inverse $-r^6$ potential was found to be quite insensitive to the specific heat ratio, γ, which recommends its use for collision number estimates of relaxing flow fields for which γ may be uncertain. Further, the inverse $-r^6$ potential was found to yield results which agreed to within approximately 20 percent of the more accurate 12:6 potential results for the entire temperature range studied. In contrast, the hard-sphere results exhibited an increasing departure from the 12:6 potential results with decreasing reservoir temperature T_o^*, which was to be expected.

In addition to providing information concerning the effects of the intermolecular potential functions on the intermolecular collision numbers in expansion flow fields, it was intended that the results be useful in the design of gas-sampling systems for both mass-sampling and optical diagnostics studies. In this regard, it was found that little advantage was afforded for the quenching of intermolecular collisions by increasing the nozzle expansion half-angle from 5 to 15 deg. Consequently, particularly for optical diagnostics applications, the expansion angle, in this range of angles, should be selected with the primary criterion of providing the desired flow-field parameters for the diagnostics system.

In conclusion, the calculations of this study can be extended easily to subsonic internal flow fields and supersonic external flows for which the Mach number-distance relationship is known.

REFERENCES

1. Hirschfelder, J. O., Curtiss, C. F. and Bird, R. B. *Molecular Theory of Gases and Liquids*. John Wiley and Sons, Inc., New York, 1964.

2. Johnston, H. S. *Gas Phase Reaction Rate Theory*. The Ronald Press Company, New York, 1966.

3. Cottrell, T. L. and McCoubrey, J. C. *Molecular Energy Transfer in Gases*. Butterworths, London, 1961.

4. Monchick, L. and Mason, E. A. "Transport Properties of Polar Gases." *J. Chem. Phys*, Vol. 35, 1961, pp. 1676-1697.

5. O'Hara, H. and Smith, F. J. "Transport Collision Integrates for a Dilute Gas." *Computer Phys. Comm.*, Vol. 2, 1971, pp. 47-54.

6. Mason, E. A. and Monchick, L. "Transport Properties of Polar-Gas Mixtures." *J. Chem. Phys.*, Vol. 36, 1962, pp. 2746-2757.

7. Williams, W. D. and Lewis, J. W. L. "Experimental Study of the Reservoir Temperature Scaling of Condensation in a Conical Nozzle Flowfield." *Progress in Astronautics and Aeronautics*, Vol. 51, Part II, 1977, pp. 1137-1151.

8. Williams, W. D. and Lewis, J. W. L. "Summary Report for the CONSET Program at AEDC." AEDC-TR-80-16 (AD-A089442), September 1980.

9. Lewis, J. W. L. and Williams, W. D. "Profile of an Anisentropic Nitrogen Nozzle Expansion.", *Phys.Fl.*, Vol. 19, 1976, pp. 951-959.

10. Young, W. S. "Correlation of Chemical Freezing in a Freejet Expansion." *AIAA J.* Vol. 13, 1975, pp. 1478-1482.
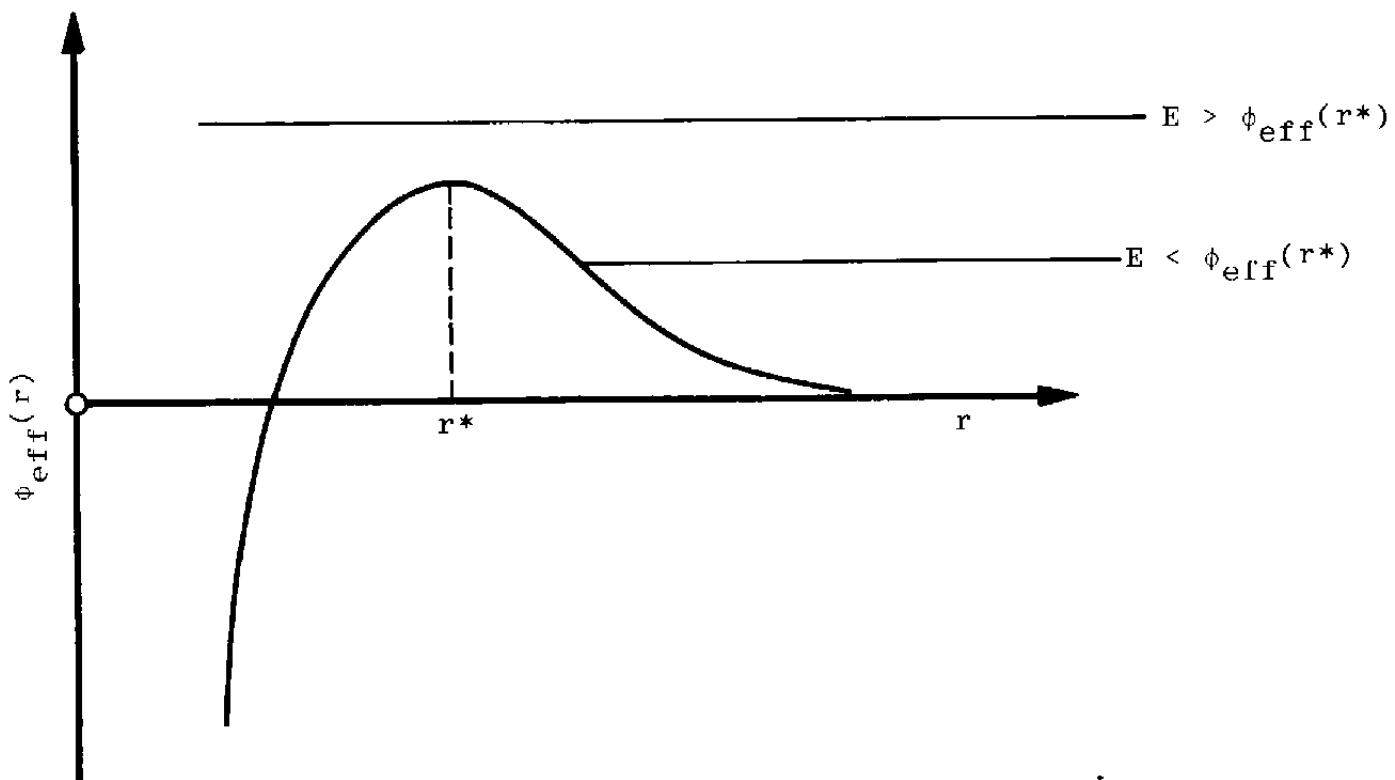
Figure 1. Radial variation of the effective potential $\phi_{eff}(r)$.
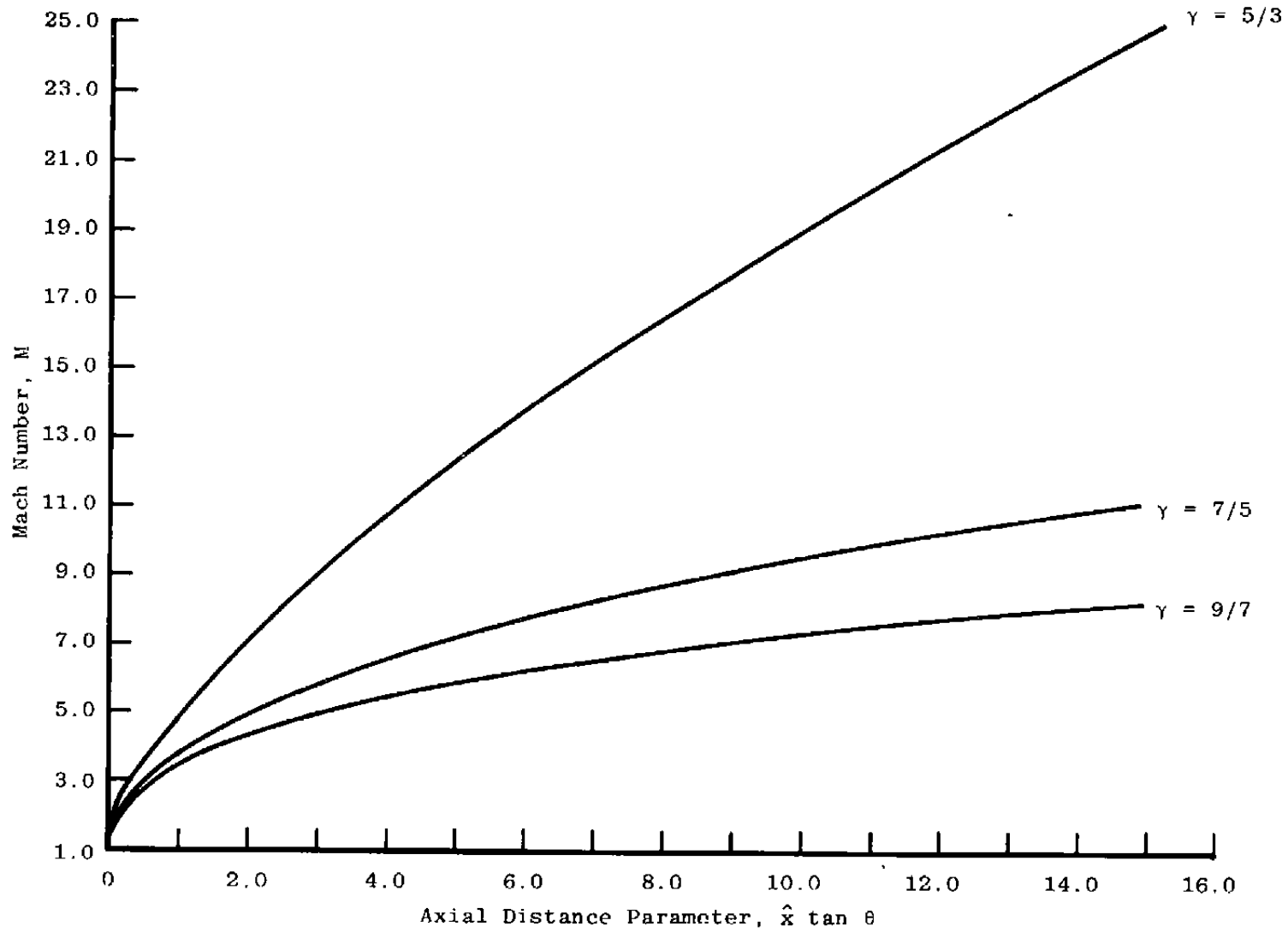
Figure 2. Variation of Mach number, M, with axial distance parameter $\hat{x} \tan \theta$.
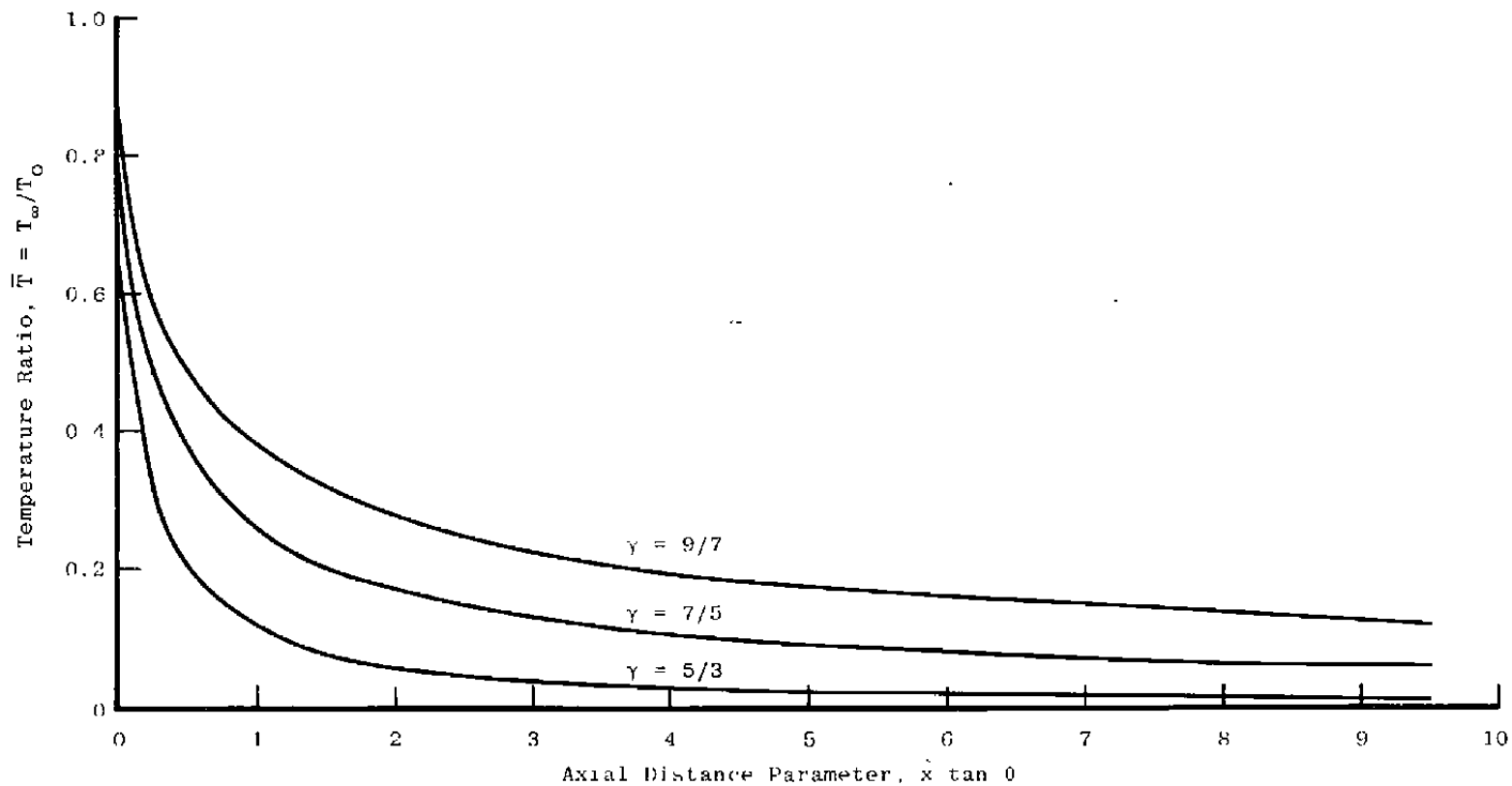
Figure 3. Variation of temperature ratio $\bar{T}$ with axial
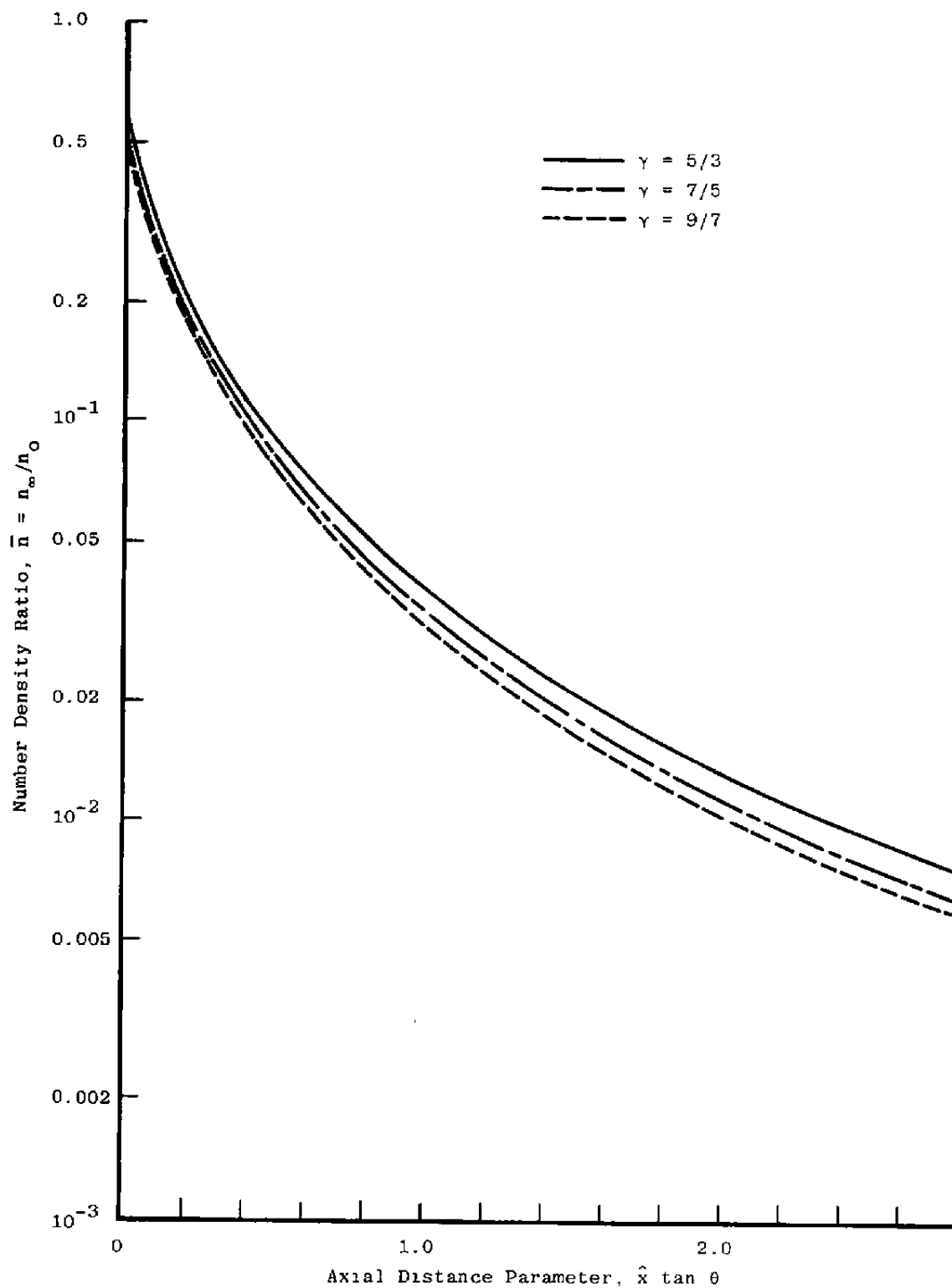distance parameter $\hat{x} \tan \theta$.

Figure 4. Variation of number density ratio $\bar{n}$ with
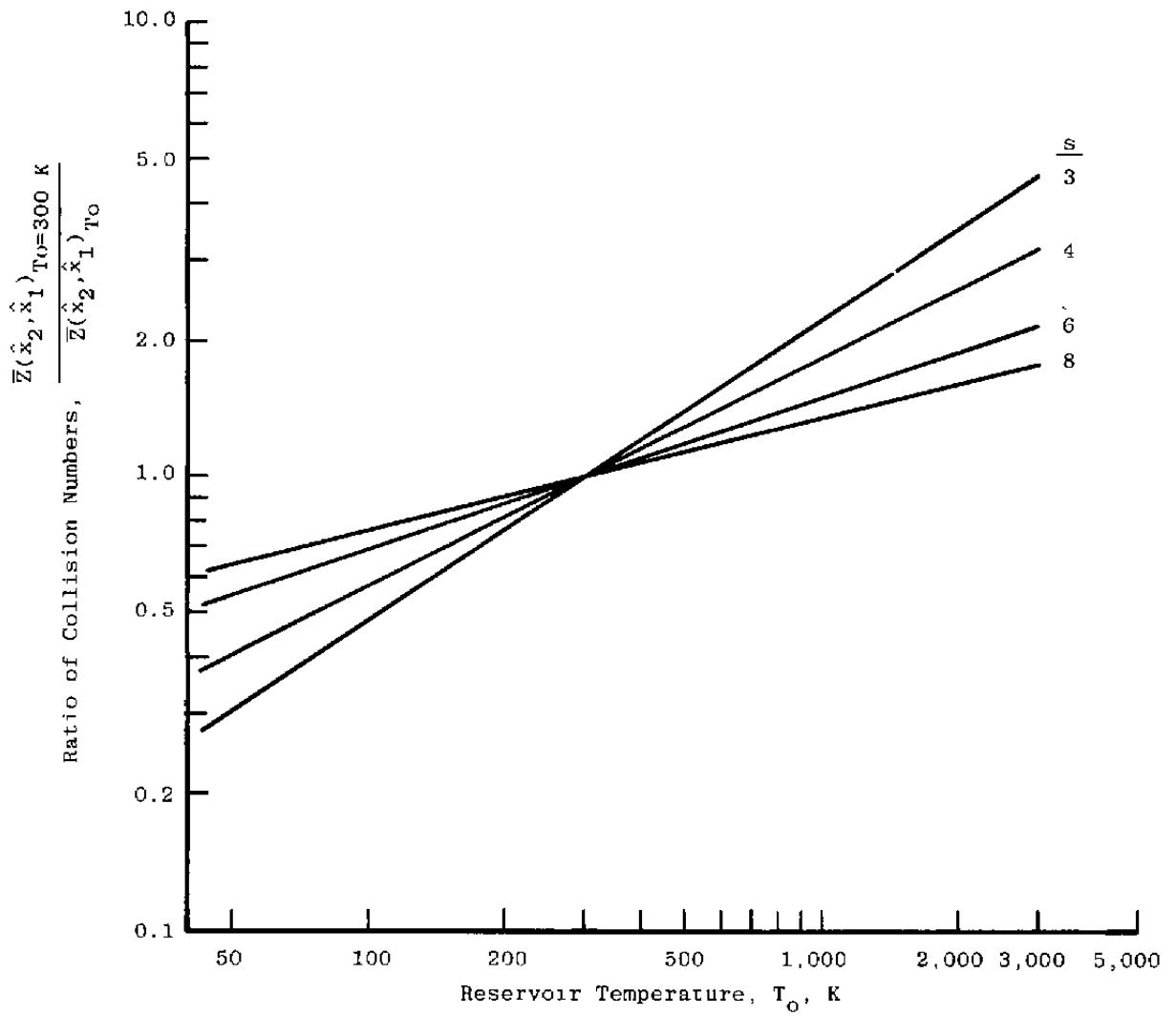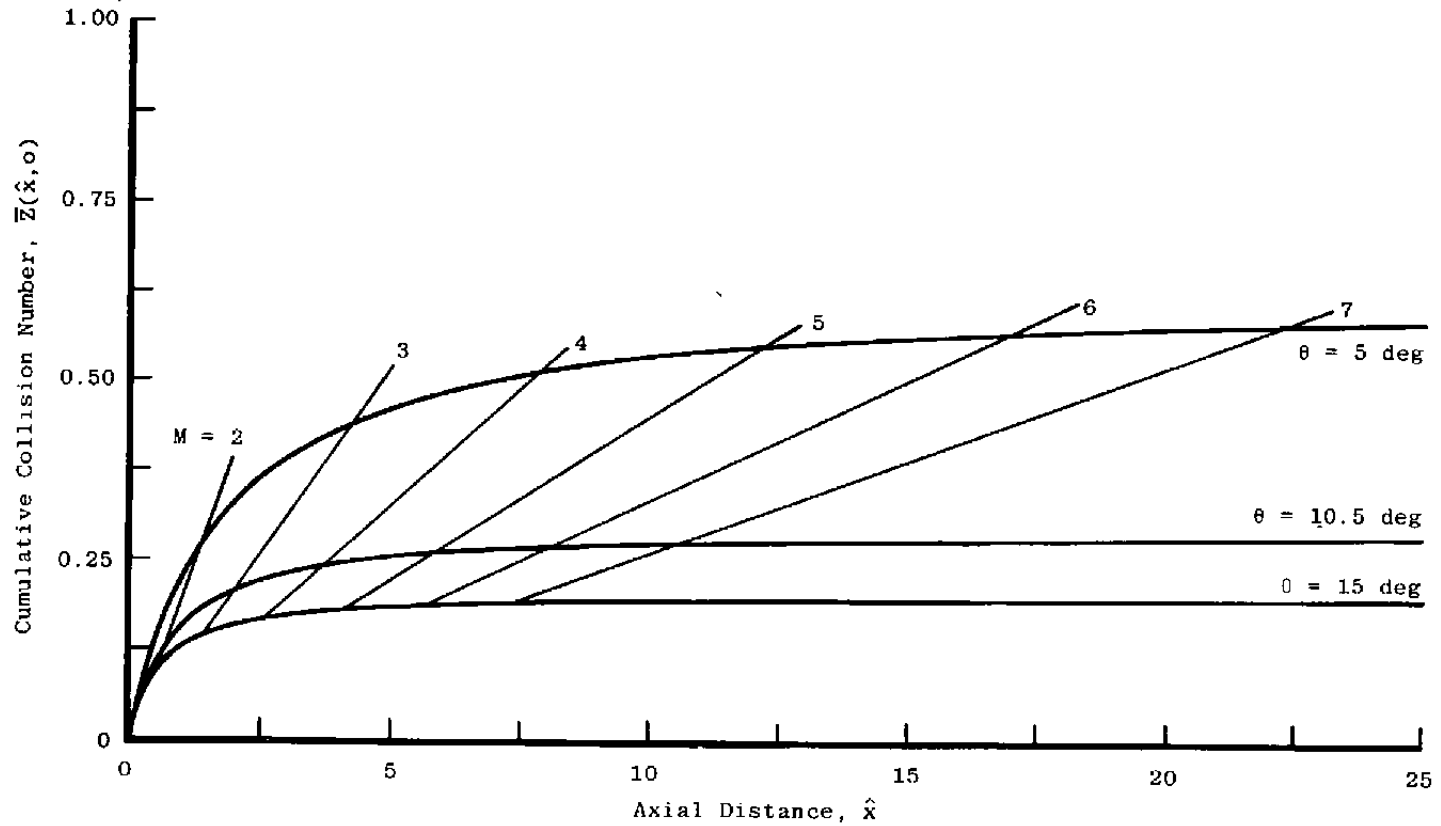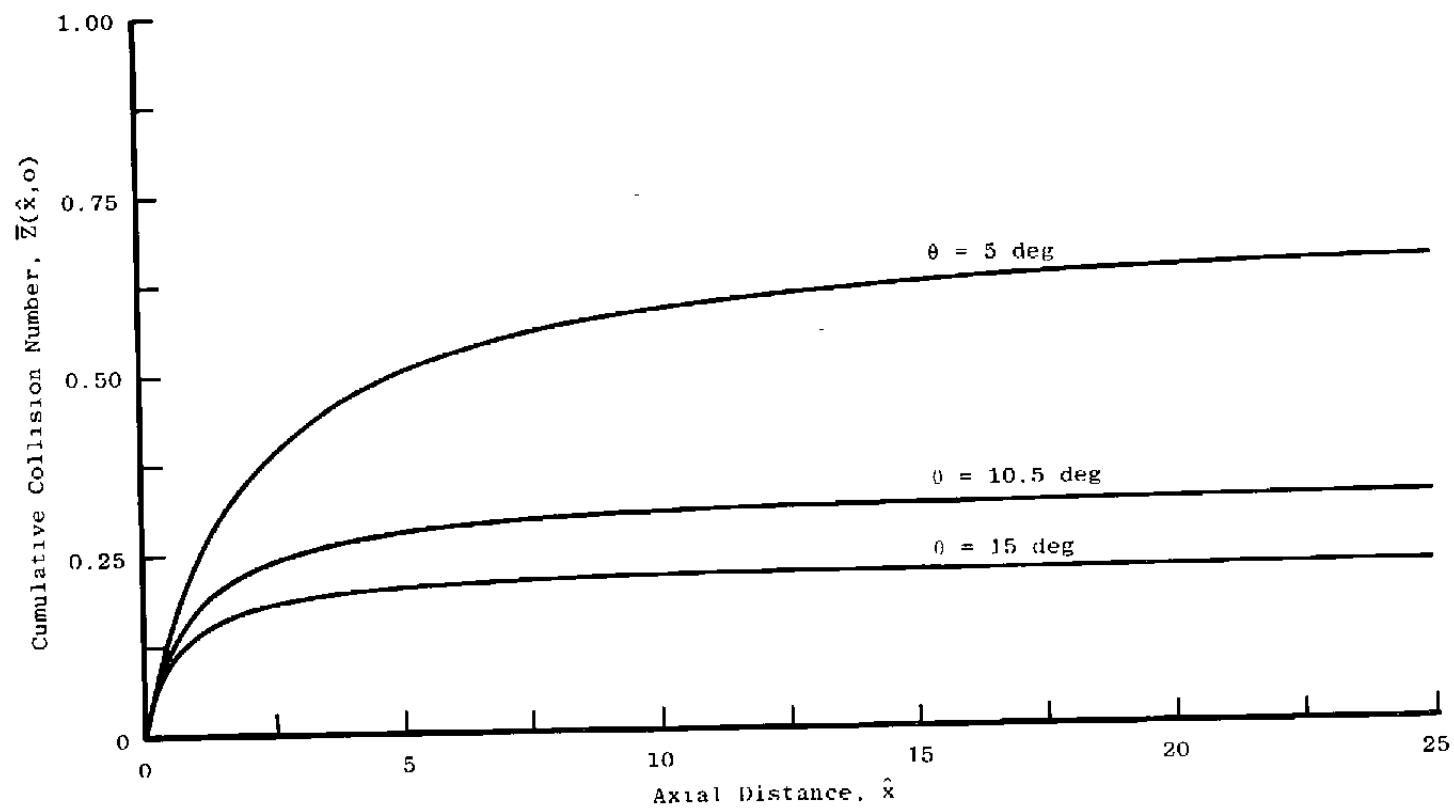axial distance parameter $\hat{x} \tan \theta$.

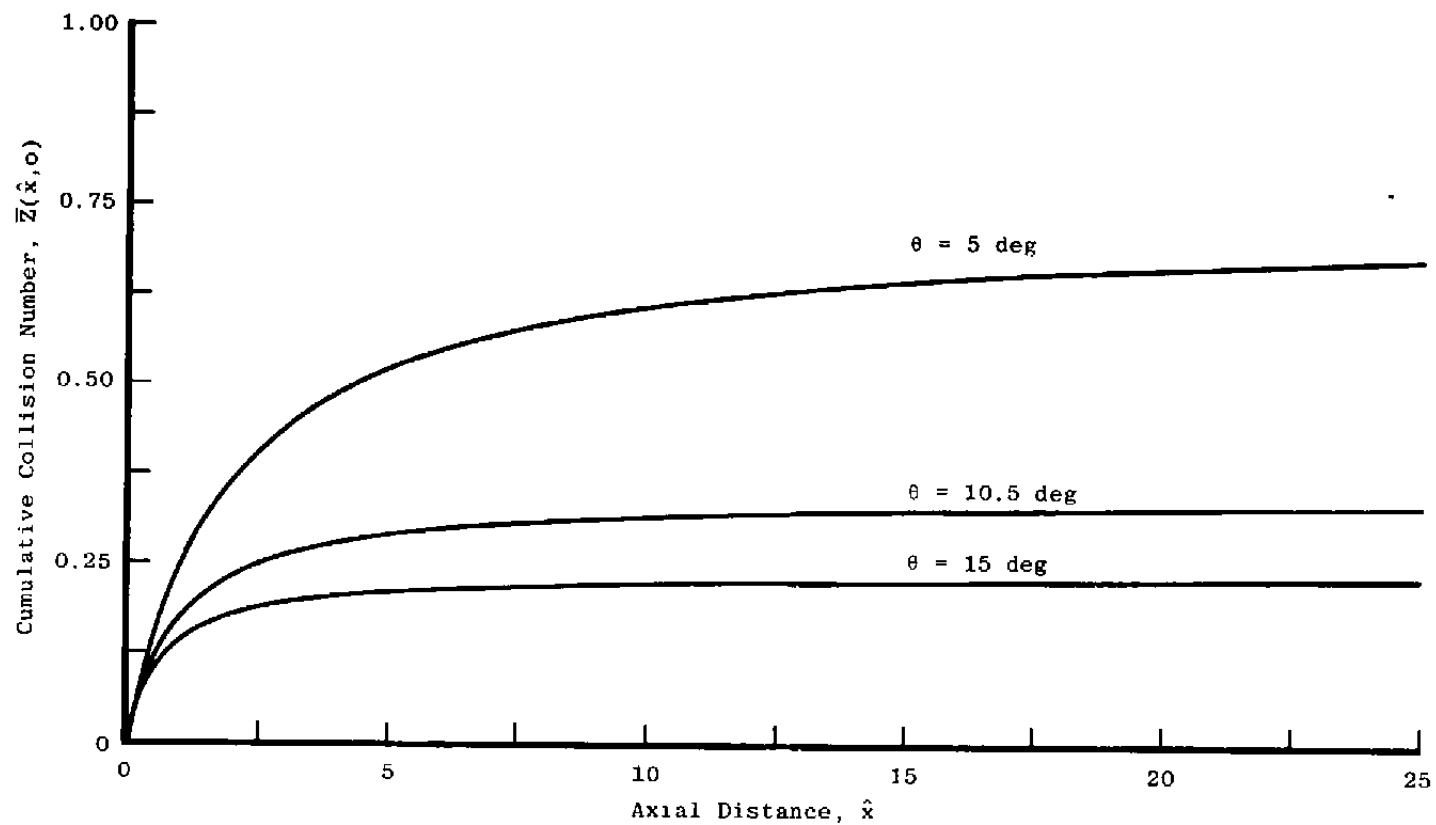Figure 5. Variation of ratio of collision numbers with reservoir temperature T_o.

a. $\gamma = 5/3$

Figure 6. Variation of the hard-sphere cumulative collision number with axial distance, $\hat{x}$, and half-angle, θ.

b. $\gamma = 7/5$
Figure 6. Continued.
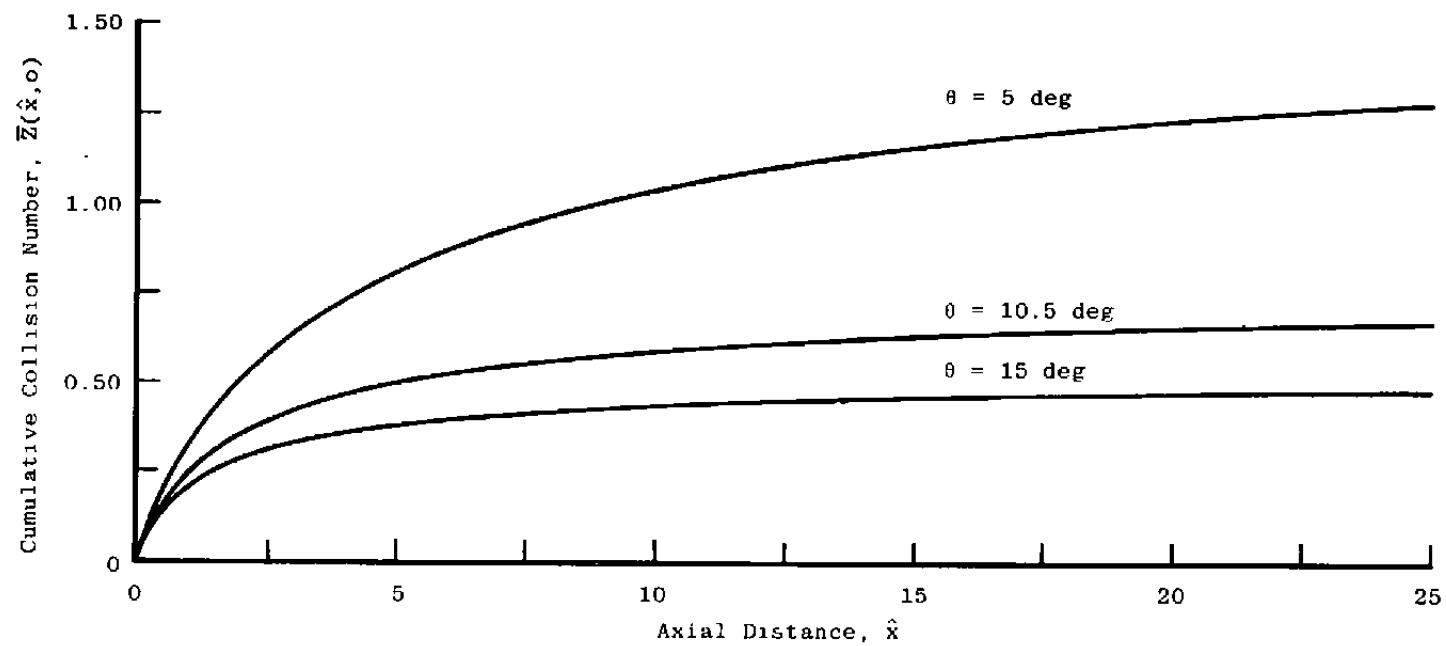
c. $\gamma = 9/7$

Figure 6. Concluded.
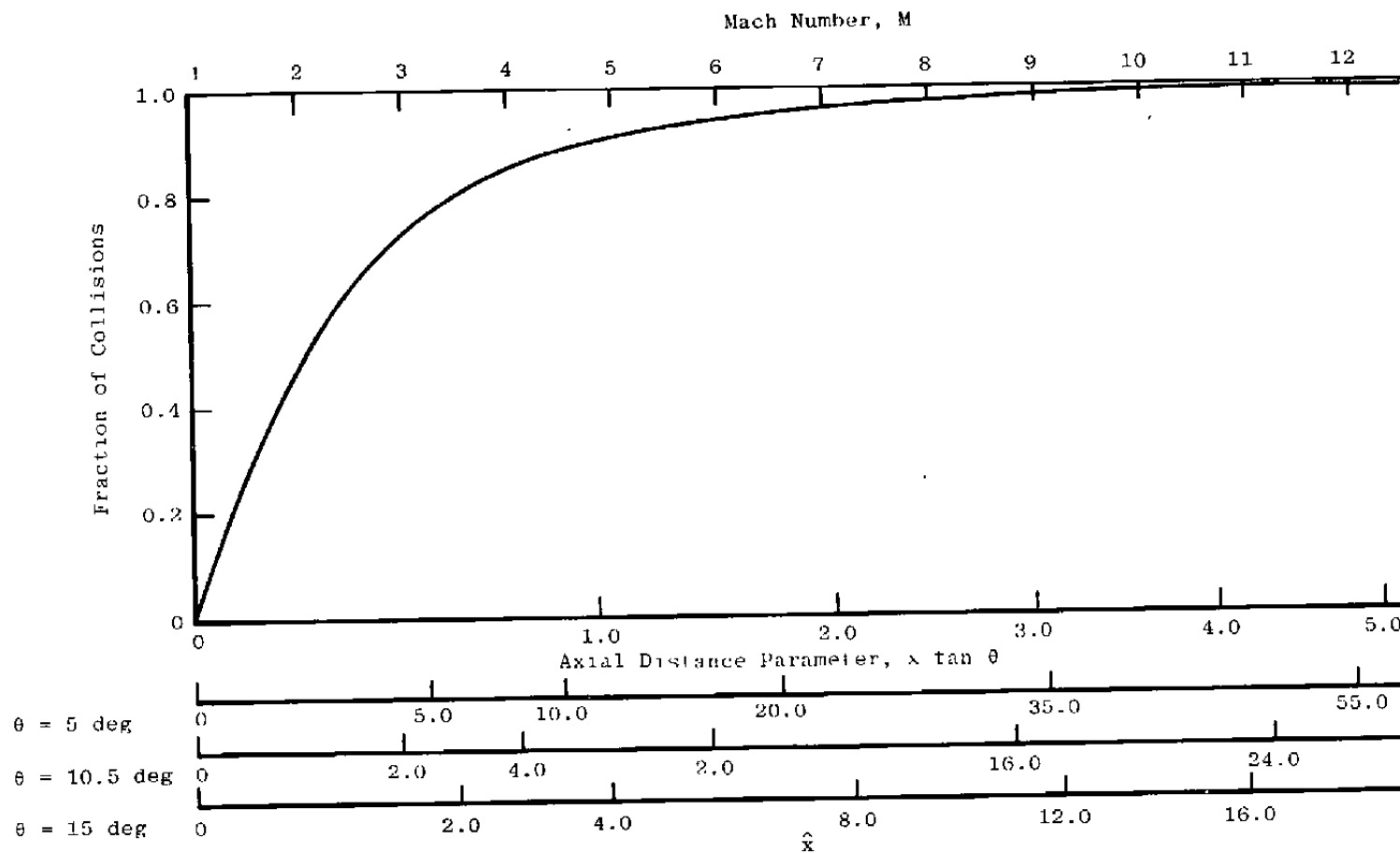
a. $\gamma = 5/3$

Figure 7. Cumulative fraction of collisions as a function of axial distance parameter, $\hat{x} \tan \theta$.
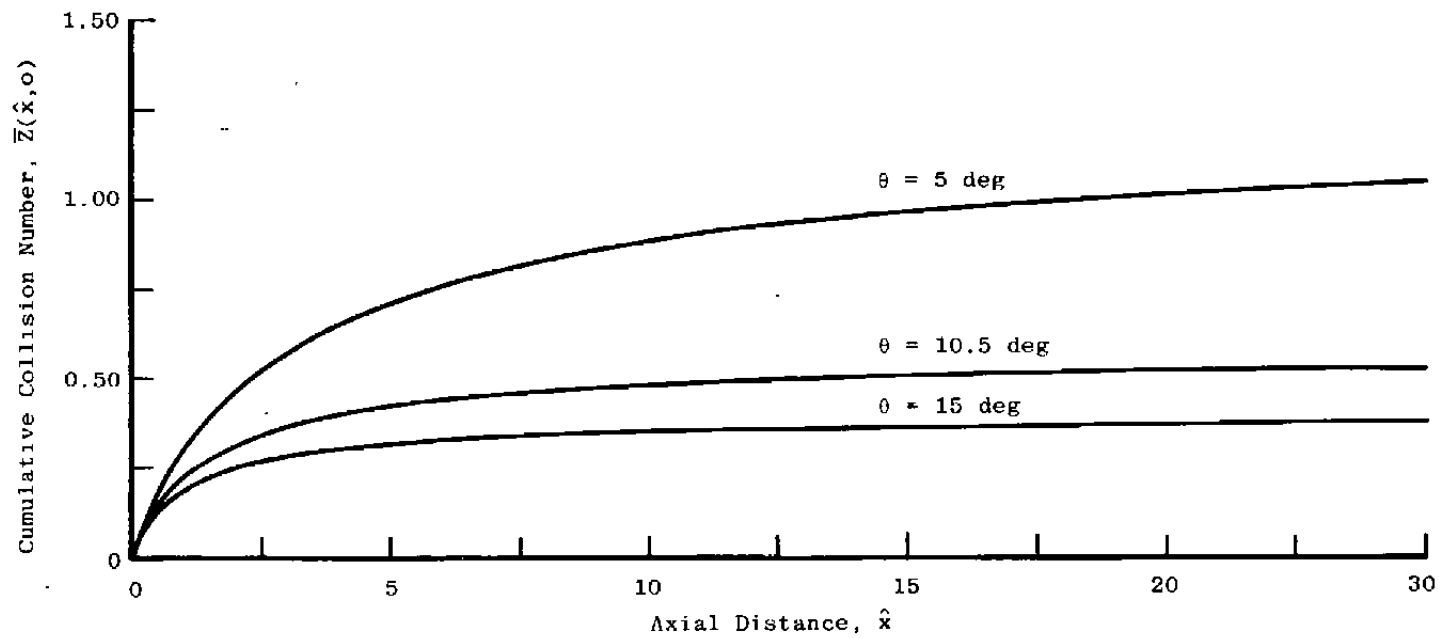
33

Mach Number, M

Fraction of Collisions

Axial Distance Parameter, $\hat{x}$ tan θ

b. γ = 7/5
Figure 7. Continued.

Mach Number, M

Fraction of Collisions

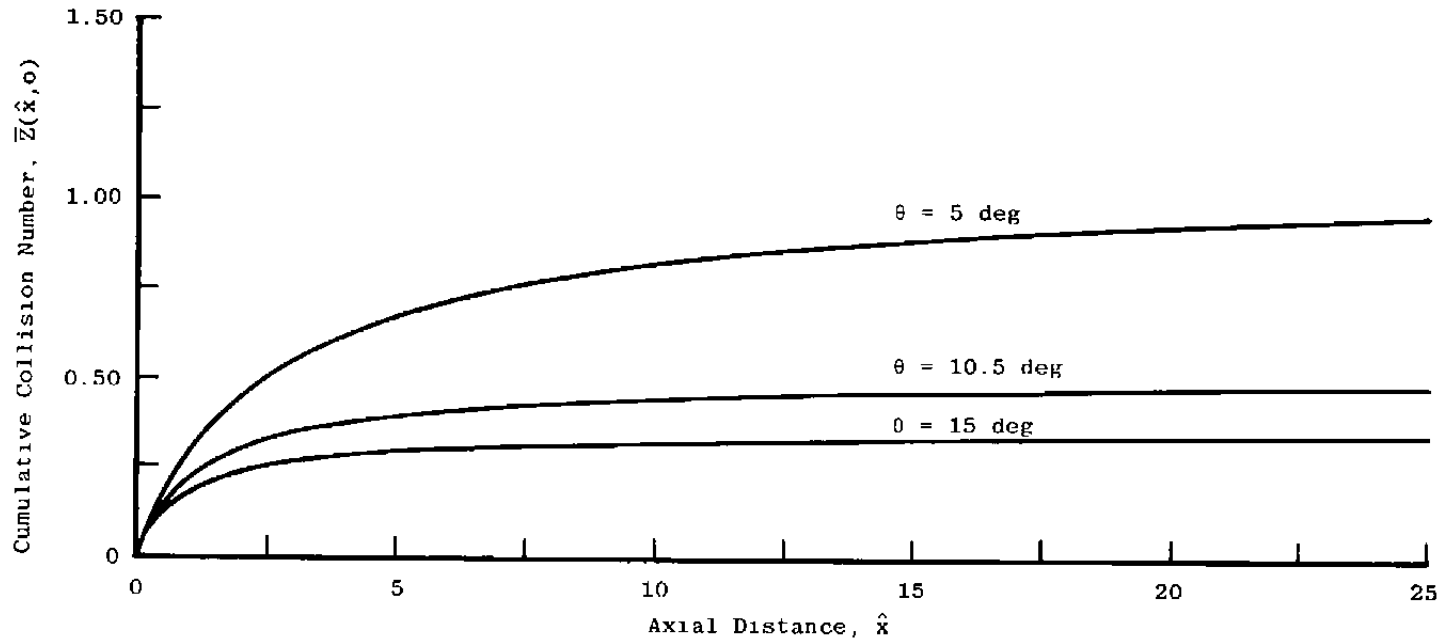Axial Distance Parameter, x tan θ
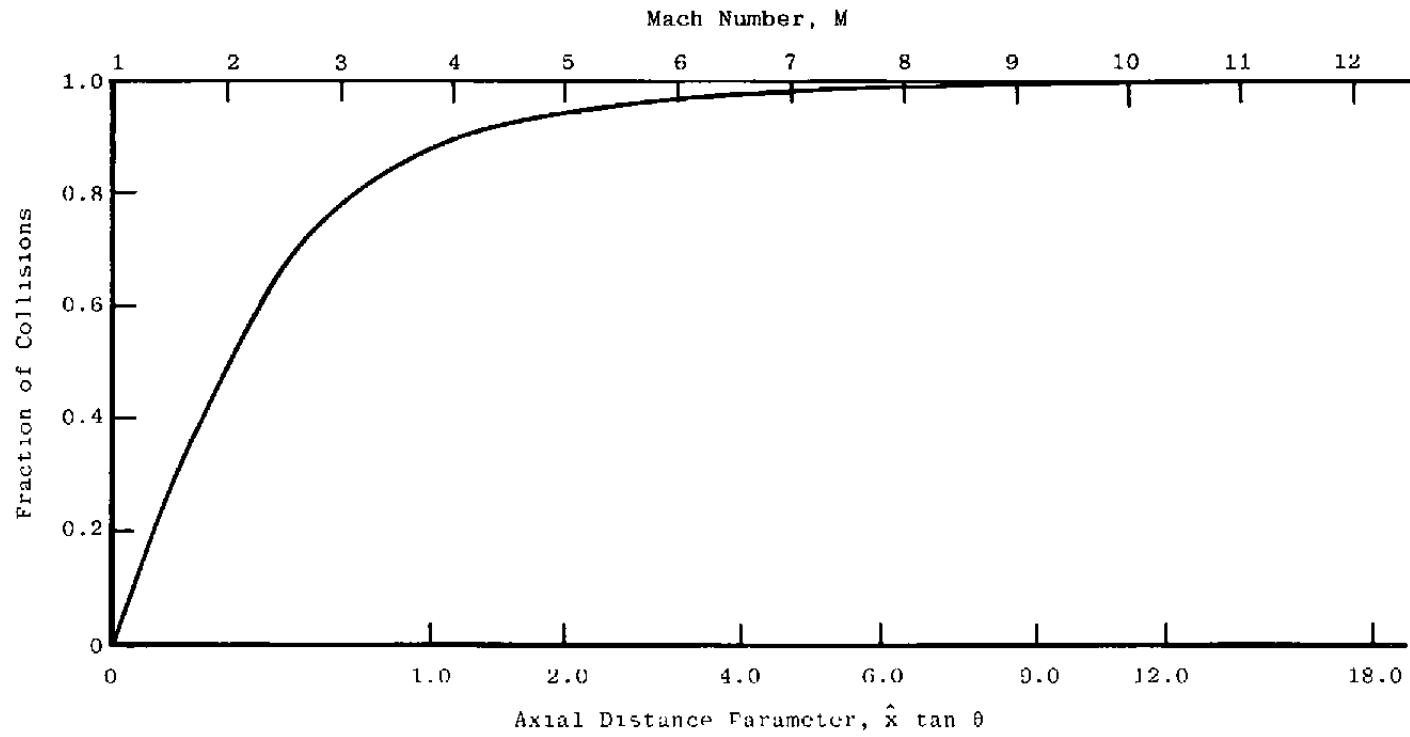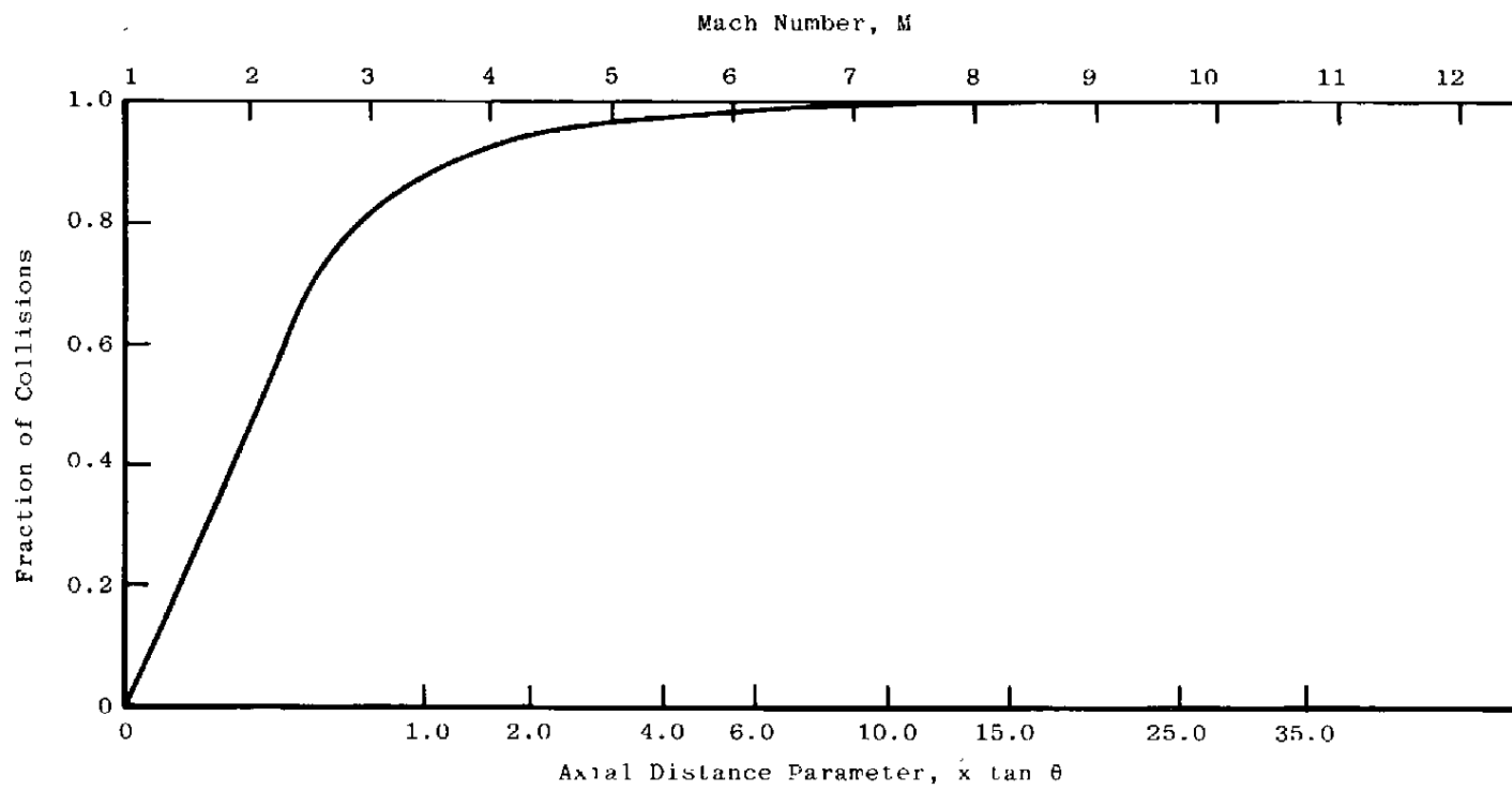
c. $\gamma = 9/7$
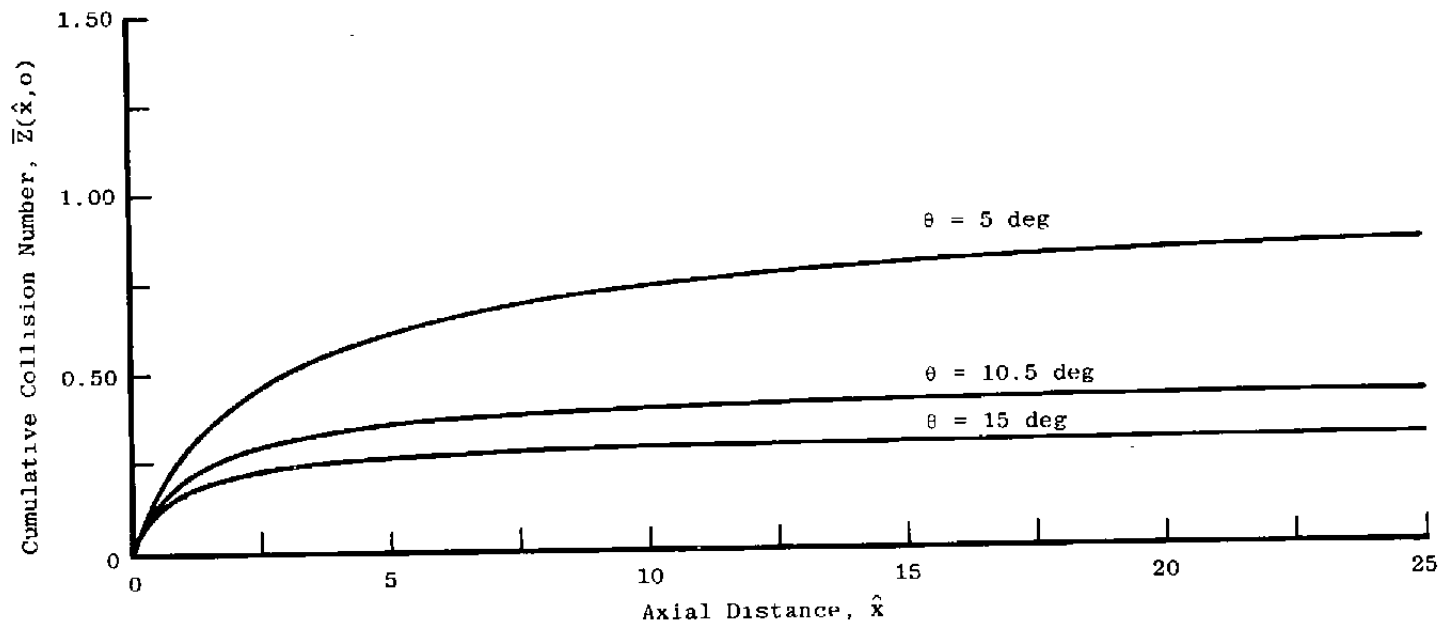
Figure 7. Concluded.

a. $\gamma = 5/3$

Figure 8. Variation of the inverse -r^3 potential cumulative collision number with axial distance, $\hat{x}$, and half-angle θ.
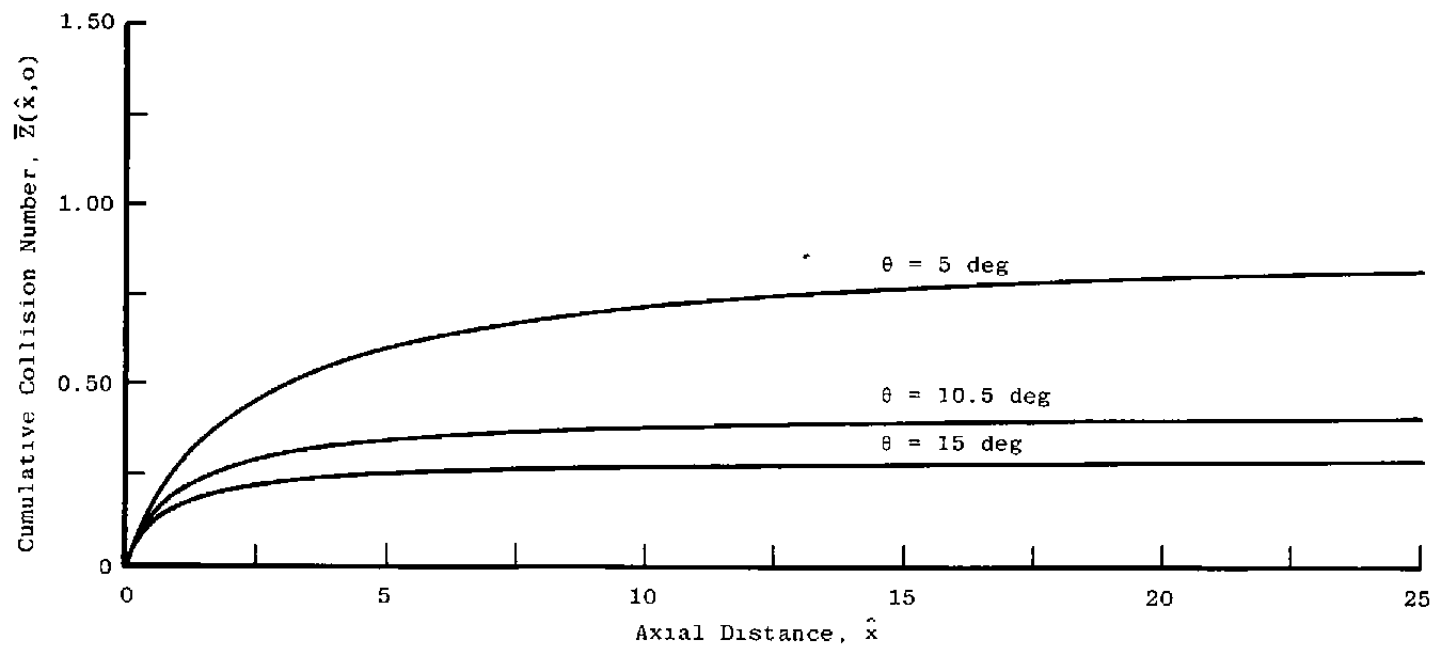
b. $\gamma = 7/5$

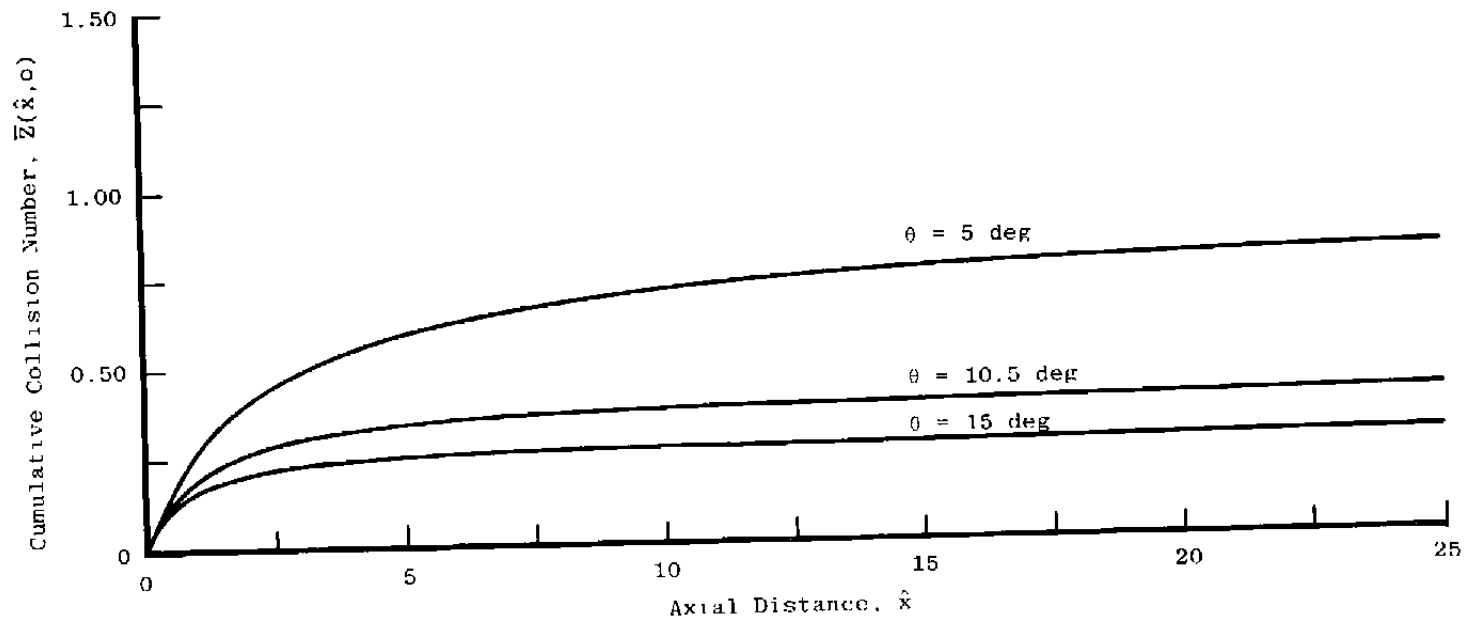Figure 8. Continued.

c. $\gamma = 9/7$
Figure 8. Concluded.
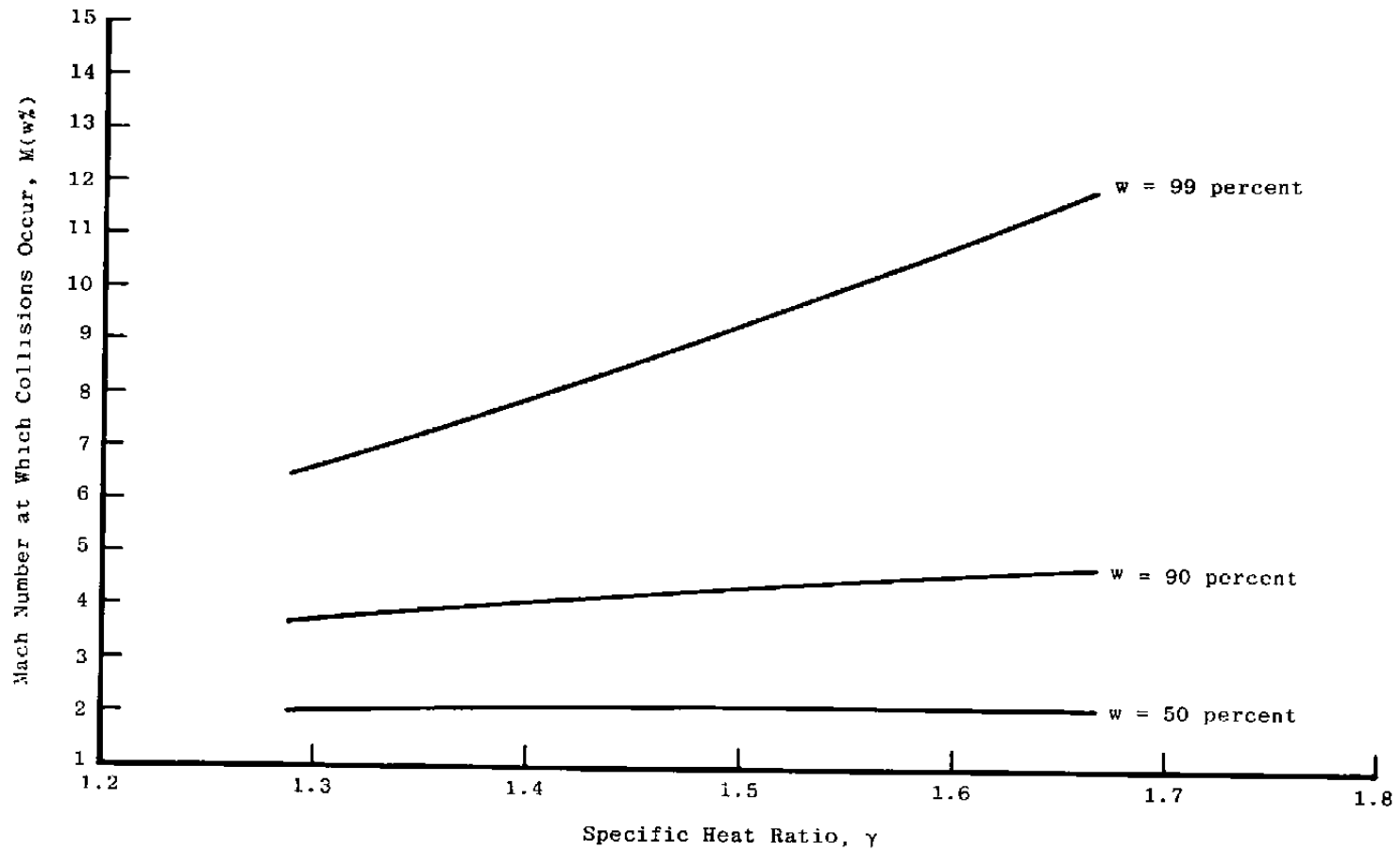
a. $\gamma = 5/3$

Figure 9. Variation of the inverse -r^6 potential cumulative collision
number with axial distance, $\hat{x}$, and half-angle, θ.

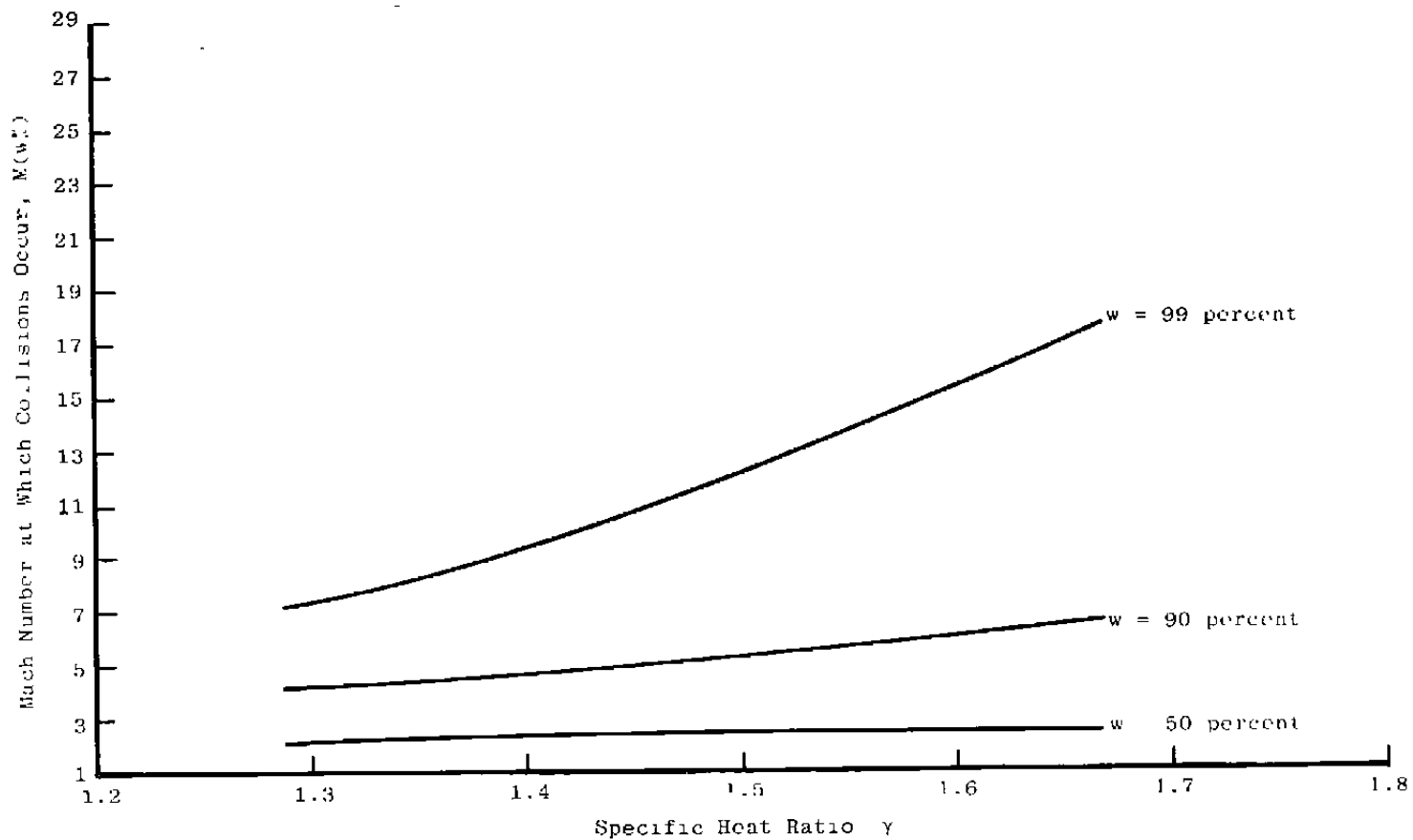b. $\gamma = 75$.
Figuire 9. Continued.

c. $\gamma = 9/7$
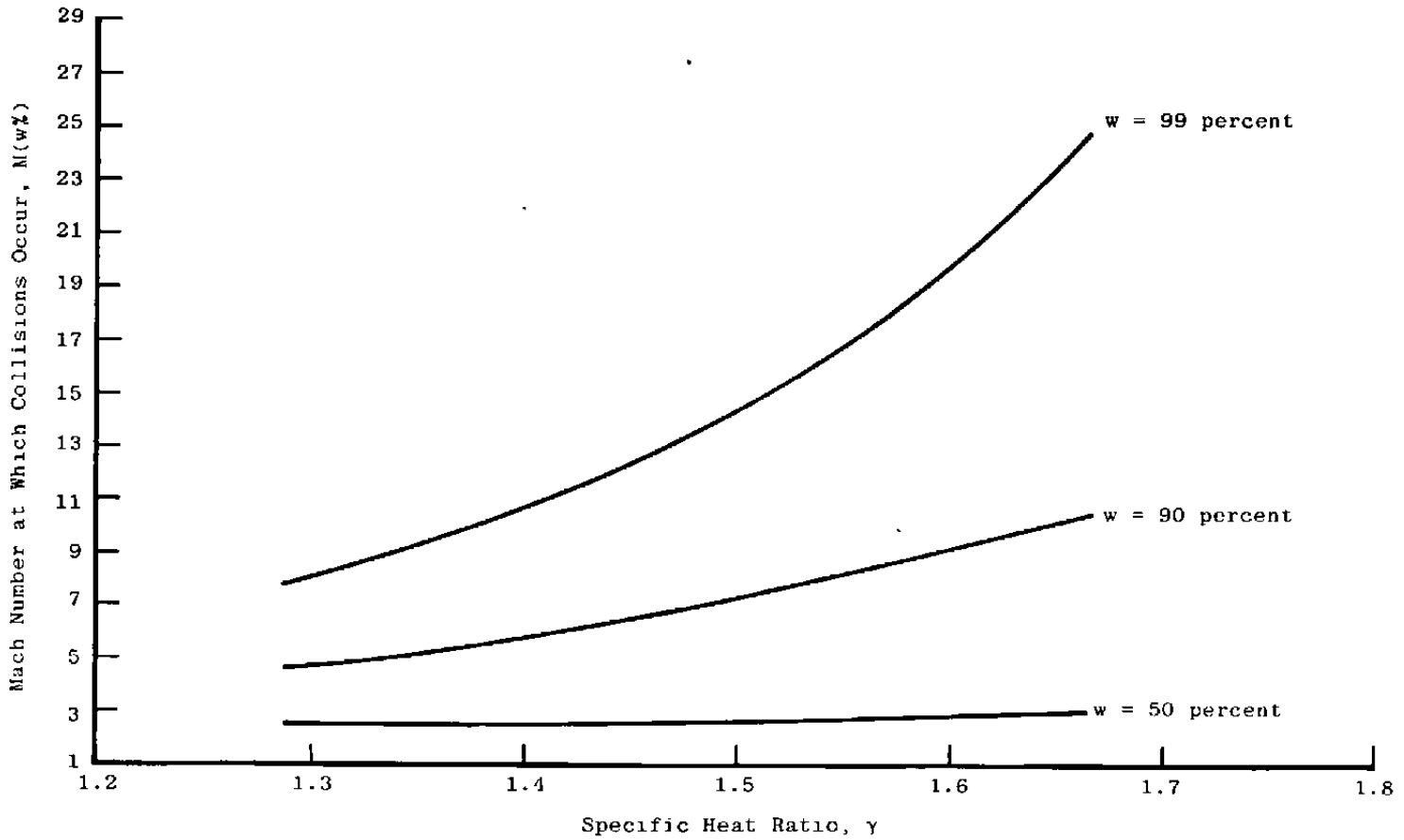Figure 9. Concluded.

a. Hard-sphere potential

Figure 10. Variation with specific heat ratio, γ, of the Mach number at which
50, 90, and 99 percent of the collisions occur.

b. Inverse -r[6] potential
Figure 10. Continued.

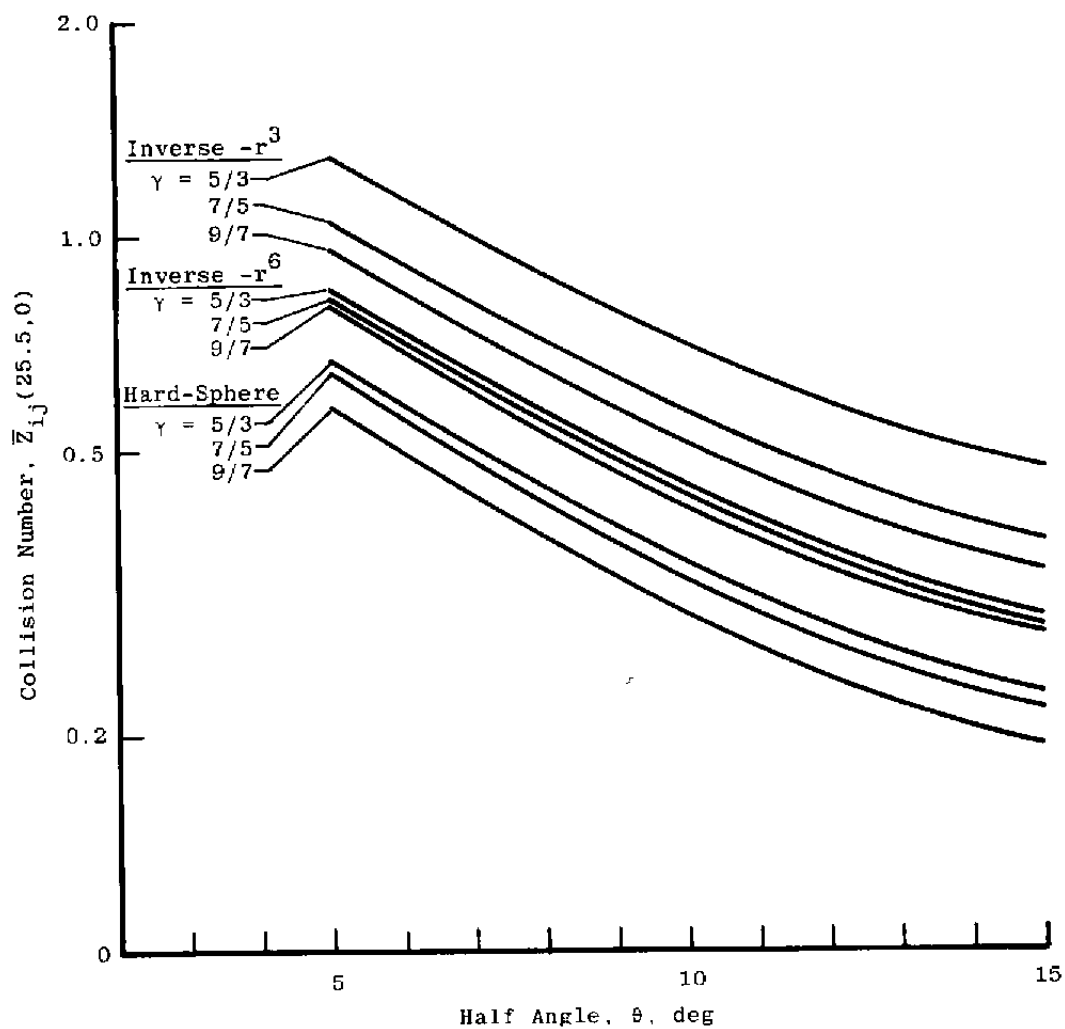c. Inverse $-r^3$ potential
Figure 10. Concluded.

Figure 11. Variation of collision number $\overline{Z}_{ij}$ (25.5, 0) with expansion half-angle, θ.
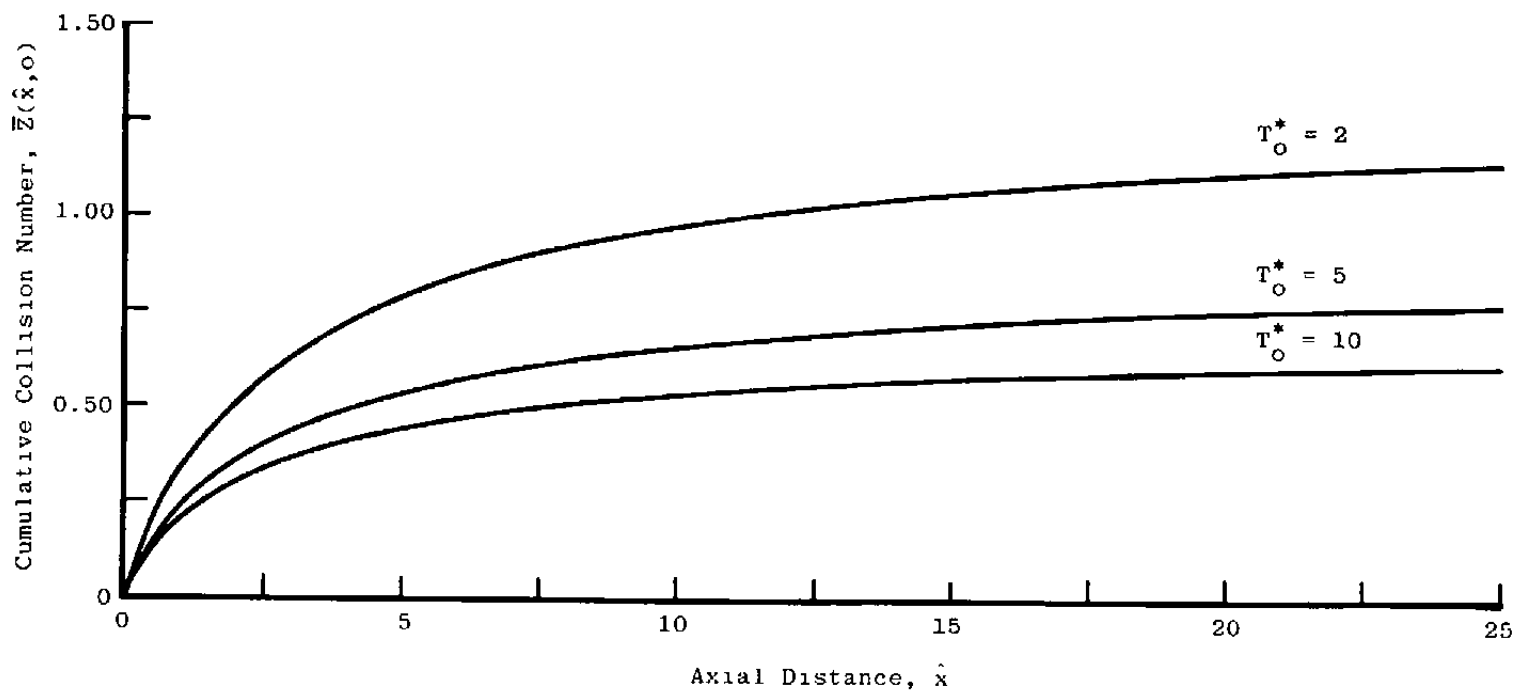
a. $\gamma = 5/3$

Figure 12. Variation of the Lennard-Jones 12:6 potential cumulative collision number with axial distance $\hat{x}$ and reservoir temperature T_o^*.
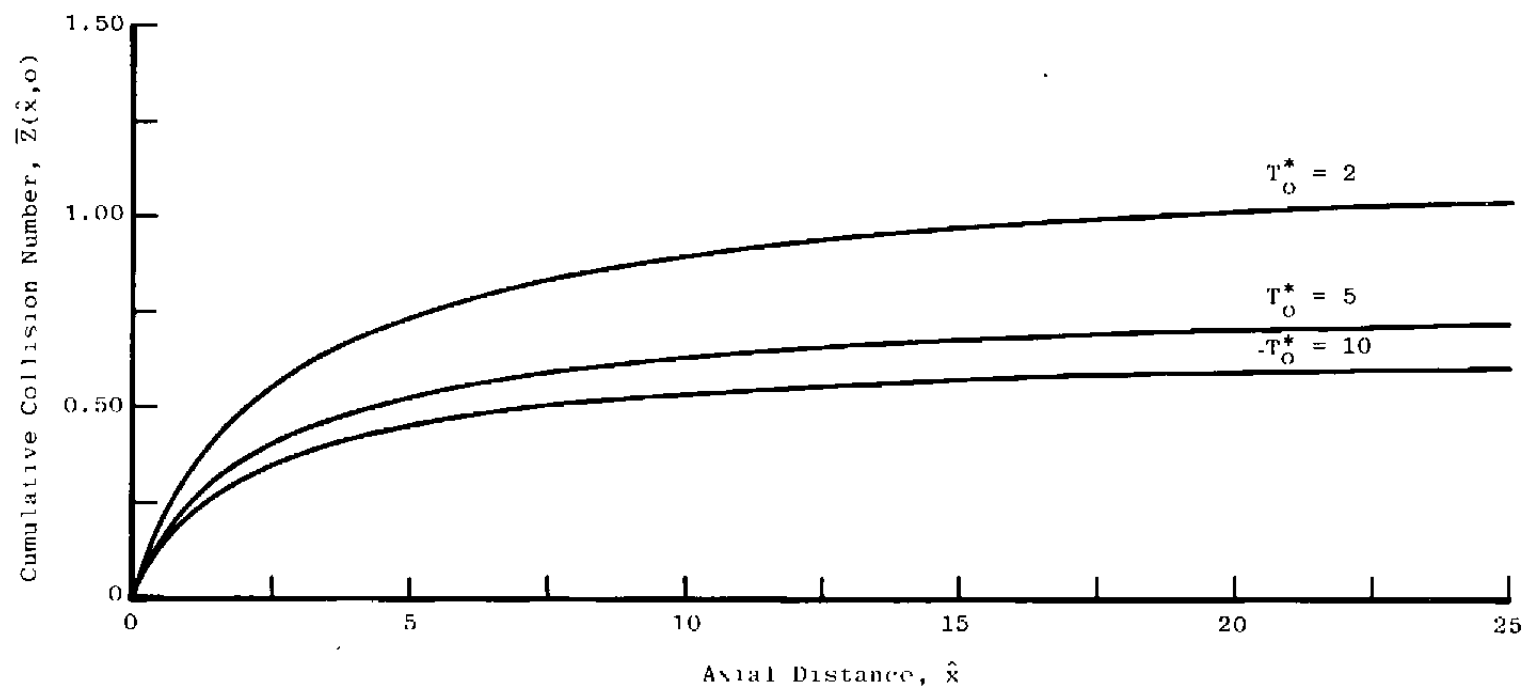
b. $\gamma = 75$
Figure 12. Continued.

c. $\gamma = 9/7$
Figure 12. Concluded.

Collision Number, $\bar{Z}_{ij}(\infty, o)$

1.2

1.0

0.8

0.6

$\gamma = 5/3$

$\gamma = 7/5$

$\gamma = 9/7$

2   5   10

2   5   10

2   5   10

Reservoir Temperature, T_o^*
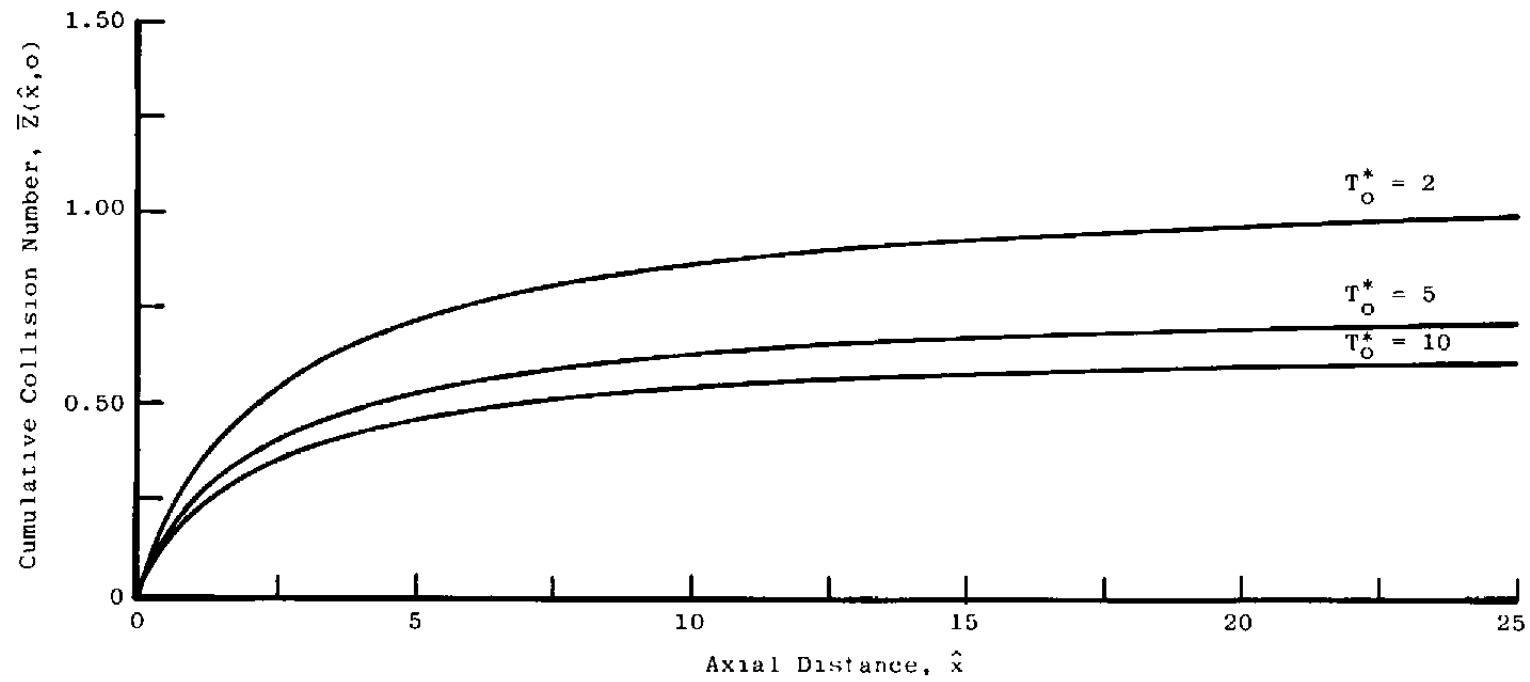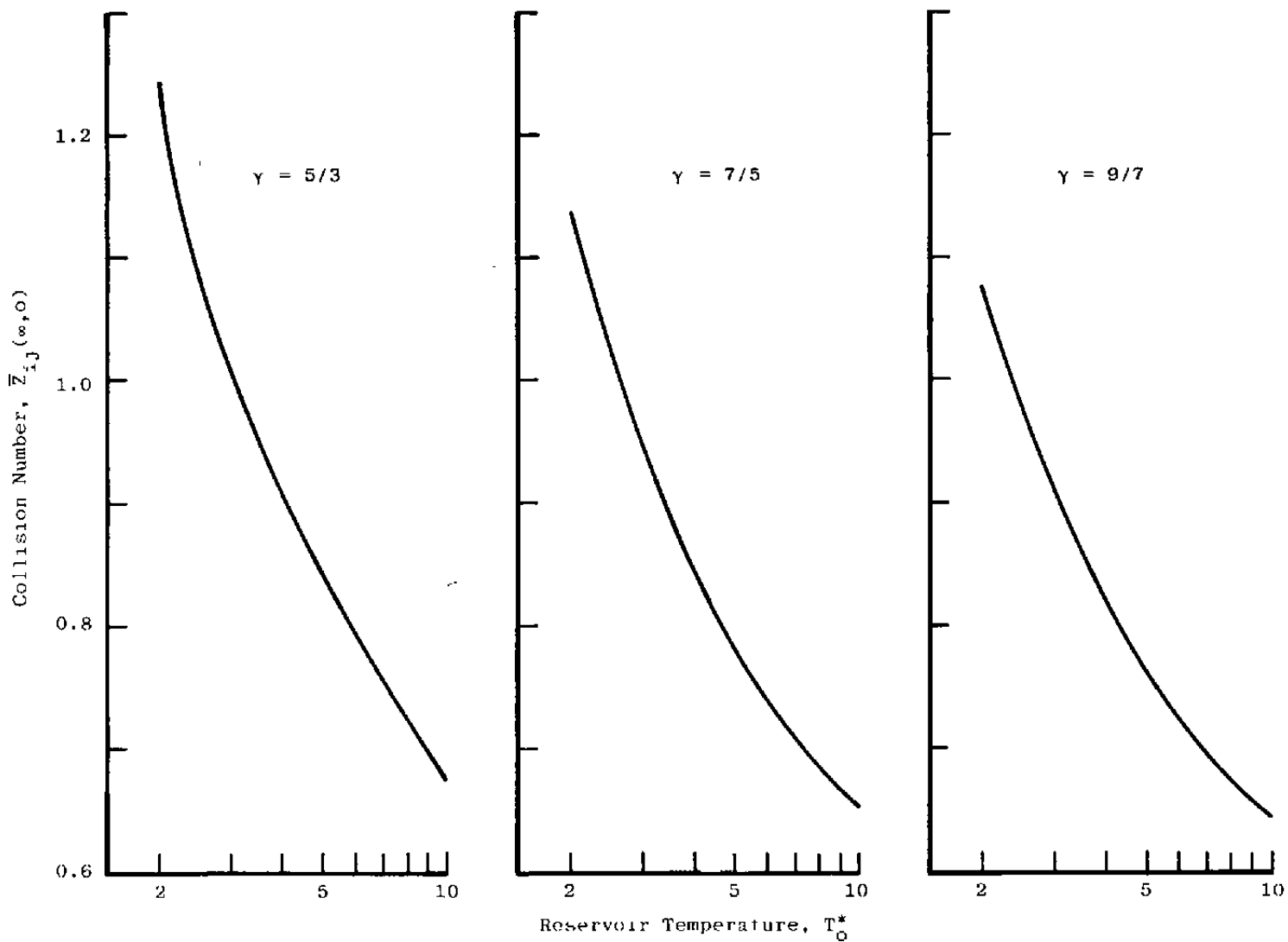
Figure 13. Variation with T_o^* of the collision number $\bar{Z}_{ij}(\infty, 0)$ for the Lennard-Jones 12:6 potential.
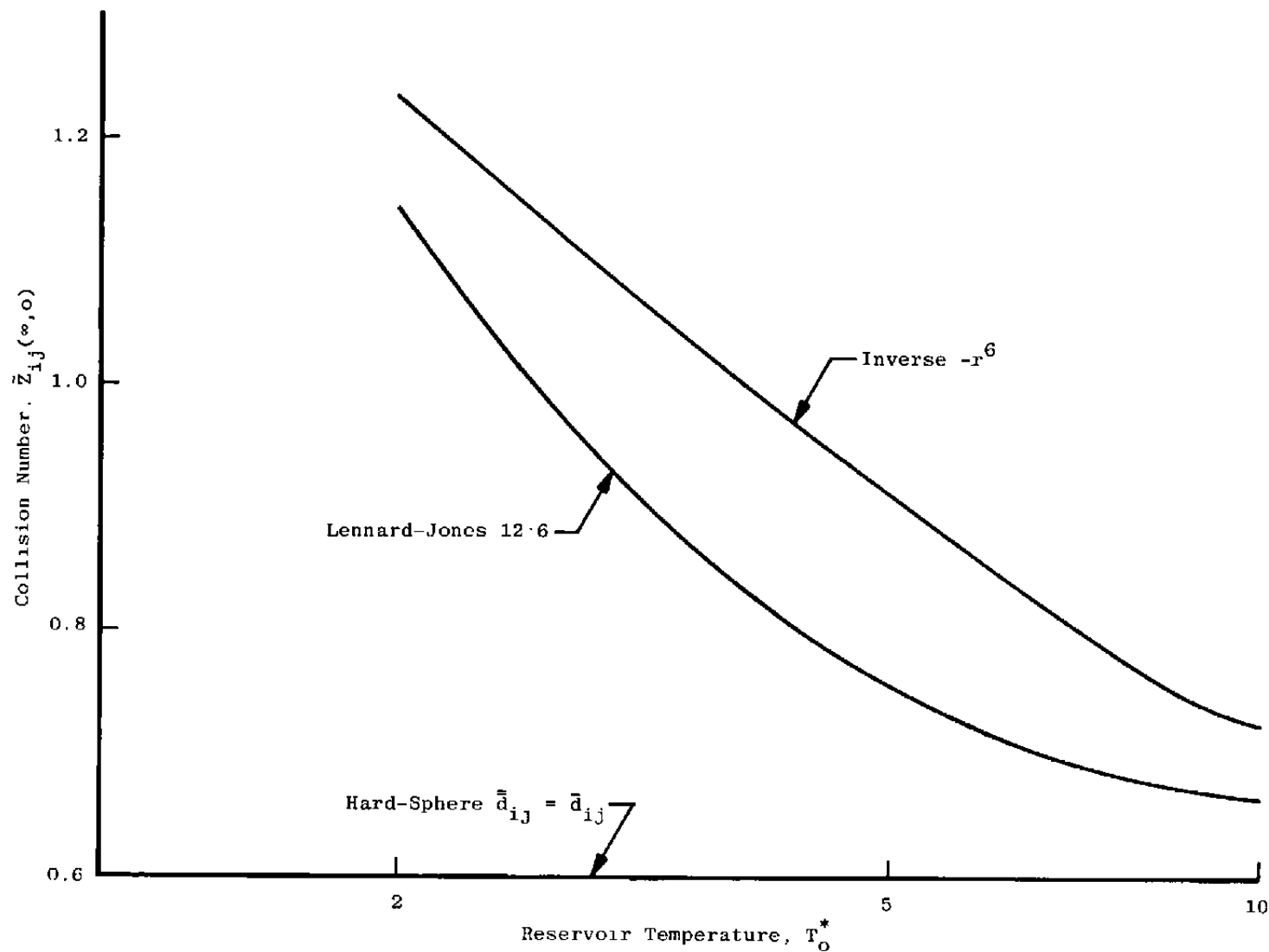
a. $\gamma = 5/3$

Figure 14. Variation with T_o^* of the collision number $\widetilde{Z}_{ij} (\infty, 0)$ for the hard-sphere, inverse $-r^6$, and Lennard-Jones 12:6 potential.

Collision Number, $\tilde{z}_{ij}(\infty, o)$

Inverse $-r^6$

Lennard-Jones 12:6

Hard-Sphere $\bar{\bar{d}}_{1J} = \bar{d}_{1J}$

Reservoir Temperature, T_o^*
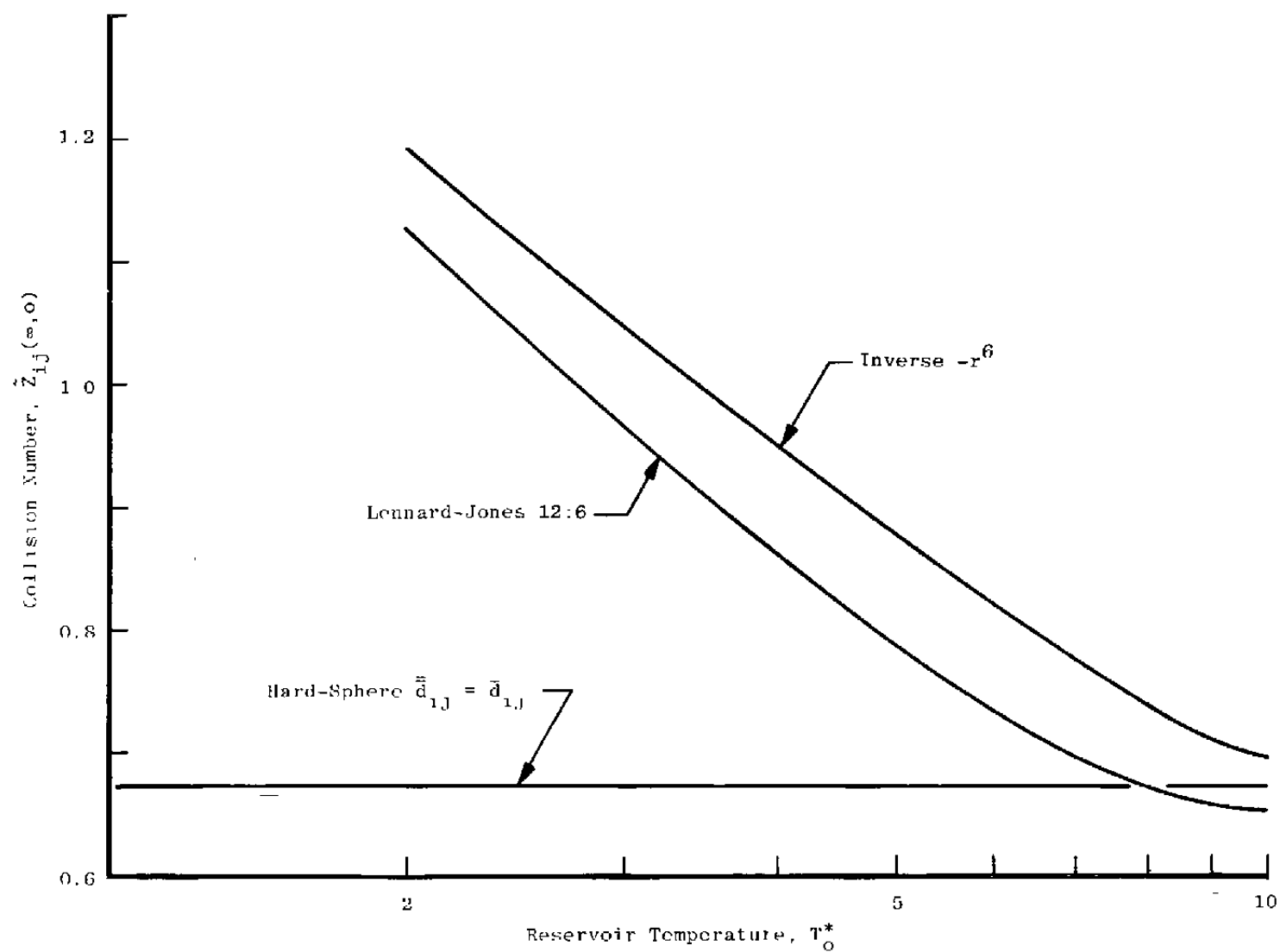
b. $\gamma = 7/5$

Figure 14. Continued.
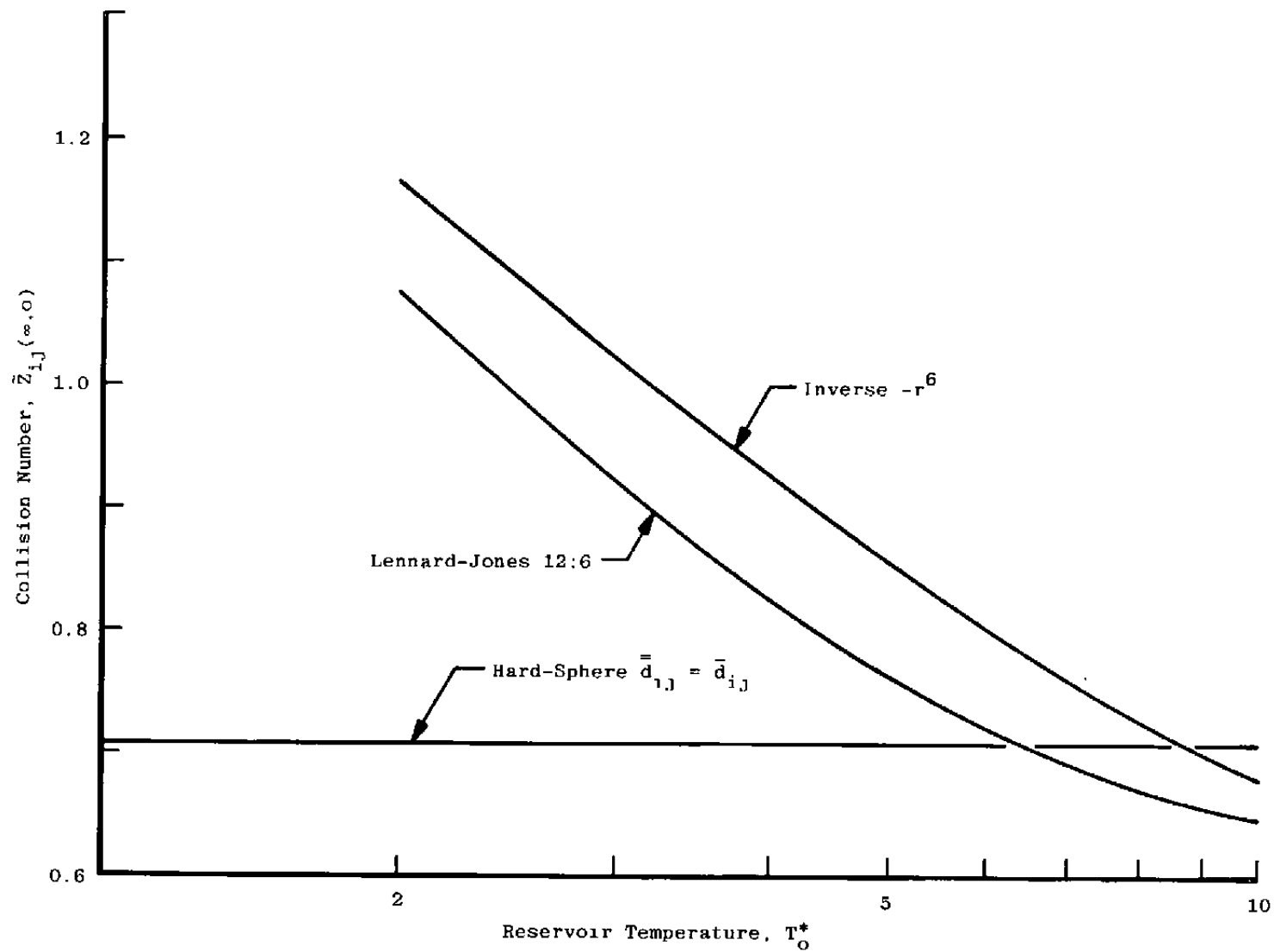
c. $\gamma = 9/7$
Figure 14. Concluded.

Figure 15. Variation of collision diameter ratio $\bar{\bar{d}}_{ij}/\bar{d}_{ij}$ with T_o^* for the inverse $-r^6$ and Lennard-Jones 12:6 potentials for γ = 5/3, 7/5, and 9/7.

Figure 16. Mach number, M, and axial distance parameter $\hat{x}$ tan θ variation of collision number $\bar{Z}_{ij}$ ($\hat{x}$, o) for polar molecules.

Table 1
Polar Gas Collision Integrals

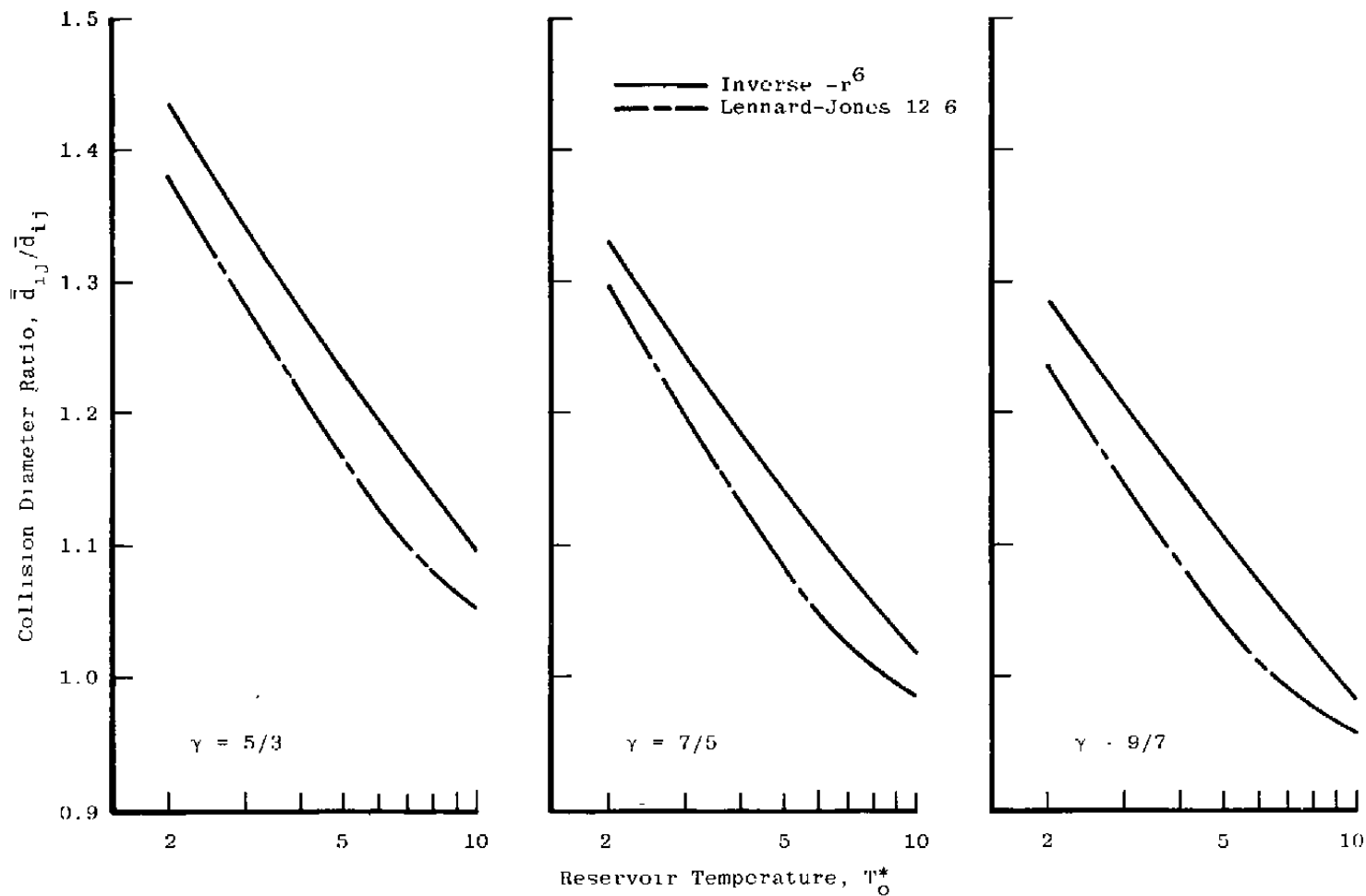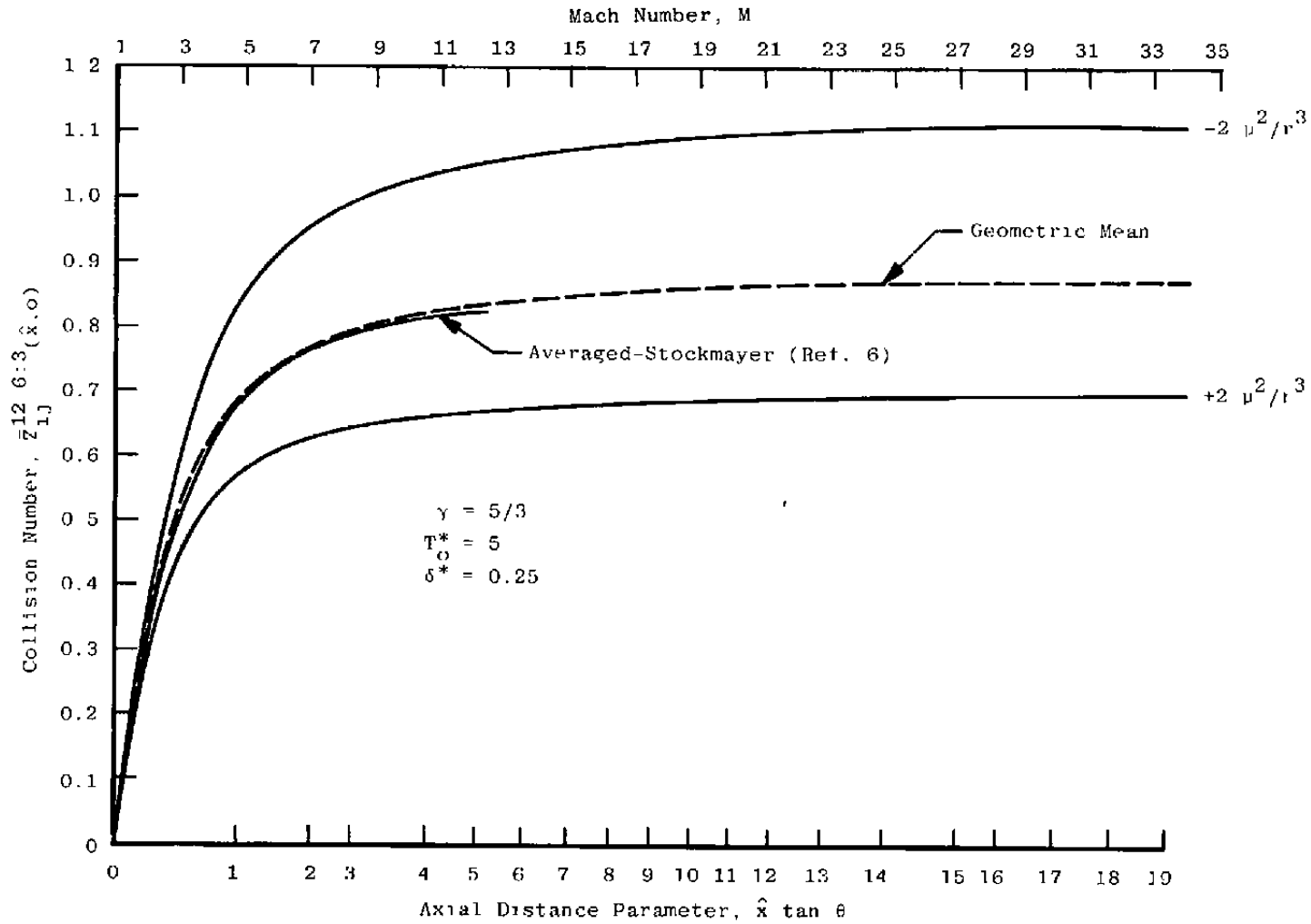| T^*	$\Omega^{(2,2)^*}_{-1}(T^*)$	$\Omega^{(2,2)^*}_{+1}(T^*)$	$\Omega^{(2,2)^*}_{gm}(T^*)$	$\Omega^{(2,2)^*}_{MM}(T^*)$	$\Omega^{(2,2)^*}_{MM}(T^*)/\Omega^{(2,2)^*}_{gm}(T^*)$
.01	29.760	21.295	25.174	---	---
.02	19.071	12.305	15.319	---	---
.03	14.802	8.482	11.205	---	---
.04	12.417	6.431	8.936	---	---
.05	10.864	5.206	7.521	---	---
.06	9.760	4.419	6.567	---	---
.07	8.927	3.885	5.889	---	---
.08	8.272	3.508	5.387	---	---
.09	7.741	3.236	5.005	---	---
0.10	7.301	3.027	4.701	4.266	0.908
0.2	5.053	2.172	3.313	3.305	0.998
0.3	4.135	1.841	2.759	2.836	1.028
0.4	3.601	1.634	2.426	2.522	1.040
0.5	3.223	1.497	2.197	2.277	1.036
0.6	2.924	1.397	2.021	2.081	1.030
0.7	2.683	1.324	1.885	1.924	1.021
0.8	2.476	1.271	1.774	1.795	1.012
0.9	2.303	1.228	1.682	1.689	1.004
1.0	2.158	1.194	1.605	1.601	0.998
1.1	2.034	1.165	1.539	1.52	0.988
1.2	1.926	1.141	1.482	1.465	0.989
1.4	1.748	1.103	1.389	1.365	0.983
1.6	1.612	1.074	1.316	1.289	0.979
1.8	1.507	1.051	1.259	1.231	0.978
2.0	1.422	1.032	1.211	1.184	0.978
2.5	1.271	0.996	1.125	1.100	0.978
3.0	1.172	0.968	1.065	1.044	0.980
3.5	1.102	0.947	1.022	1.044	1.022
4.0	1.052	0.929	0.989	0.9732	0.942
5.0	0.982	0.900	0.940	0.9291	0.988
6.0	0.936	0.878	0.907	0.8979	0.990
7.0	0.903	0.859	0.881	0.8741	0.992
8.0	0.877	0.843	0.860	0.8549	0.994
9.0	0.856	0.830	0.843	0.8388	0.995
10.0	0.839	0.818	0.828	0.8251	0.996
12.0	0.812	0.798	0.805	0.8024	0.997
14.0	0.791	0.781	0.786	0.7840	0.977
16.0	0.774	0.767	0.770	0.7687	0.998
18.0	0.759	0.754	0.756	0.7554	0.999
20.0	0.747	0.743	0.745	0.7438	0.998
25.0	0.721	0.720	0.721	0.7200	0.999
30.0	0.702	0.701	0.702	0.7011	0.999

NOMENCLATURE

$\bar{\bar{a}}$	Strength of interaction
b	Impact parameter
b_c	Critical impact parameter
D	Orifice or throat diameter
D_{ij}^{*}	$D/\bar{d}_{ij}$
d	Collision diameter
$\bar{d}_{ij}$	Characteristic range parameter
$\bar{\bar{d}}$	Hard-sphere collision diameter
E	Energy
F	Function equal to $\{1 + [(\gamma-1)/2]M^2\}$
f(v)	Velocity distribution function
g	Function defined by Eq. (27c)
K	Rate coefficient
k_B	Boltzmann's constant
M	Mach number
$\overline{M}_i$	Gram molecular weight of species i
$<\overline{M}>$	Gram molecular weight of mixture gas
M_{ij}	Reduced mass gram molecular weight
m_i	Mass of species i molecule
$\bar{m}$	Reduced mass of collision
$\bar{m}_{ij}$	Reduced mass of species i and j defined by Eq. (13d)
N_A	Avogadro's number
n	Number density
n^*	Dimensionless number density defined by Eq. (33b)

R	Universal gas constant
r	Intermolecular separation distance
s	Potential index
T	Temperature
T*	Dimensionless temperature $T/(\epsilon/k_B)$
t	Time
u_∞	Flow speed
v	Speed
X_i	Mole fraction of species i
x	Flow-field axial distance
$\hat{x}$	x/D
Z_{ij}	Cumulative collision number for species i molecule attributable to collisions with species j molecule
$\bar{Z}$	Nondimensional cumulative collision number defined by Eqs. (26a), (27a), (27c), and (32a)
$\tilde{Z}$	Nondimensional cumulative collision number defined by Eqs. (36), (37), and (38)
$\hat{Z}$	Collision frequency
$\hat{\hat{Z}}$	Collision frequency per unit volume
α_s	Parameter defined by Eq. (38)
$\Gamma(x)$	Gamma function of x
γ	Specific heat ratio
δ^*	Parameter defined by Eq. (34b)
ϵ	Characteristic energy
ζ	Dipole alignment parameter
η	Viscosity

θ	Nozzle half-angle
$\bar{\theta}$	Spherical polar angle of alignment of dipole moment
μ	Dipole moment
ξ	Species identity factor
σ	Cross section
ϕ	Potential
$\bar{\phi}$	Azimuthal angle of alignment of dipole moment
$\Omega^{(1,s)*}$	Collision integral

SUBSCRIPTS

c	Center of mass; critical
eff	Effective
gm	Geometric mean
MM	Monchick-Mason
o	Reservoir parameter
r	Relative velocity
T	Total value
α,i,j	Species type
ζ	Dipole alignment parameter
∞	Free-stream parameter

SUPERSCRIPTS

12:6	Parameter appropriate to Lennard-Jones 12:6 potential
12:6:3	Parameter appropriate to 12:6:3 potential
HS	Hard-sphere
s	Parameter appropriate to inverse $-r^s$ power potential